MABS
2025, VOL. 17, NO. 1, 2479531
https://doi.org/10.1080/19420862.2025.2479531

Taylor & Francis
Taylor & Francis Group

REPORT

OPEN ACCESS Check for updates

Design of orthogonal constant domain interfaces to aid proper heavy/light chain pairing of bispecific antibodies

Kyle A. Barlow[a], Michael B. Battles[b], Michael E. Brown[c], Kaleigh Canfield[d], Xiaojun Lu[c], Heather Lynaugh[c], Morgan Morrill[d], C. Garrett Rappazzo[e], Saira P. Reyes[e*], Chanita Sandberg[d], Beth Sharkey[d], Christin Strong[d], Jingfu Zhao[c], and Arvind Sivasubramanian[a,e]

[a]Computational Biology, Adimab, Mountain View, CA, USA; [b]Antibody Engineering, Adimab, Lebanon, NH, USA; [c]Protein Analytics, Adimab, Lebanon, NH, USA; [d]High-Throughput Expression, Adimab, Lebanon, NH, USA; [e]Platform Technologies, Adimab, Lebanon, NH, USA

ABSTRACT

The correct pairing of cognate heavy and light chains is critical to the efficient manufacturing of IgG-like bispecific antibodies (bsAbs) from a single host cell. We present a general solution for the elimination of heavy chain (HC):light chain (LC) mispairs in bsAbs with κ LCs via the use of two orthogonal constant domain (C_H1:Cκ) interfaces comprising computationally designed amino acid substitutions. Substitutions were designed by Rosetta to introduce novel hydrogen bond (H-bond) networks at the C_H1:Cκ interface, followed by Rosetta energy calculations to identify designs with enhanced pairing specificity and interface stability. Our final design, featuring a total of 11 amino acid substitutions across two Fab constant regions, was tested on a set of six IgG-like bsAbs featuring a diverse set of unmodified human antibody variable domains. Purity assessments showed near-complete elimination of LC mispairs, including in cases with high baseline mispairing with wild-type constant domains. The engineered bsAbs broadly recapitulated the antigen-binding and biophysical developability properties of their monospecific counterparts and no adverse immunogenicity signal was identified by an in vitro assay. Fab crystal structures containing engineered constant domain interfaces revealed no major perturbations relative to the wild-type coordinates and validated the presence of the designed hydrogen bond interactions. Our work enables the facile assembly of independently discovered IgG-like bispecific antibodies in a single-cell host and demonstrates a streamlined and generalizable computational and experimental workflow for redesigning conserved protein:protein interfaces.

ARTICLE HISTORY
Received 13 December 2024
Revised 6 March 2025
Accepted 10 March 2025

KEYWORDS
Bispecific antibodies; antibody engineering; heavy chain/light chain pairing; computational protein design; in vitro developability assay; developability

Introduction

The US Food and Drug Administration (FDA) issued its first bispecific antibody approval, for blinatumomab (Blincyto), in 2014. In the decade since, at least 17 additional bispecific antibodies (bsAbs) have received regulatory approval worldwide (db.antibodysociety.org).[1,2] The majority of these (11/17) are bsAbs[3–5] with a natural IgG-like architecture. IgG-like bsAbs bind monovalently to two distinct antigens or epitopes, with each specificity encoded in the variable domains of one antigen-binding fragment (Fab) arm via correct pairing of heavy and light chains. Unlike alternative formats, IgG-like bsAbs are likely to inherit favorable attributes related to biophysical developability and industrial manufacturing of the IgG class, and are thus an attractive option for therapeutics.[2]

A correctly assembled four-chain IgG-like bispecific composed of two distinct light and heavy chains requires the formation of three heterodimeric interfaces: one formed by two distinct heavy chain (HC) Fc domains and two Fab heterodimers formed by the cognate pairing of the heavy and light chains (LCs). Without the presence of strong driving forces, random-chain interactions cause the formation of heavy-chain homodimers and incorrect pairings between light and heavy chains. This process results in a heterogeneous mixture containing up to 10 possible species: the correctly assembled bispecific molecule and nine unintended side products.[2]

Efficient manufacturing of bsAbs requires approaches to either address or circumvent the significant challenge of chain mispairing. In FDA-approved IgG-like bsAbs, diverse technologies have been used to enable the preferential formation of heavy-chain heterodimers over homodimers (HC:HC pairing) along with the correct pairing of heavy chains with their respective cognate light chains (HC:LC pairing).[6] Technologies to optimize HC pairing[2] include purification of heterodimers via isoelectric point (pI) engineering (e.g., emicizumab), preferential heterodimer formation via Knob-in-Hole (KiH) amino acid (AA) substitutions (e.g., mosunetuzumab and faricimab), and controlled Fab Arm Exchange (cFAE) (e.g., amivantamab, epcoritamab, and teclistamab).[2,6] HC:LC pairing, the focus of this work, has been addressed using different molecular formats such as tandem scFv (blinatumomab) and CrossMab.[2,7] Common Light Chain (cLC) bispecific antibodies (e.g., emicizumab) can be discovered using both in vitro[8–10] and in vivo[11–13] methods, but cannot readily be used to combine independently discovered sets of variable

CONTACT Arvind Sivasubramanian arvind.sivasubramanian@adimab.com Computational Biology, Adimab, 444 Castro St, Mountain View, CA 94041, USA
*My present affiliation for Saira P. Reyes: Department of Bioengineering, Stanford University, Stanford, CA, USA.
Supplemental data for this article can be accessed online at https://doi.org/10.1080/19420862.2025.2479531

© 2025 Adimab LLC. Published with license by Taylor & Francis Group, LLC.
This is an Open Access article distributed under the terms of the Creative Commons Attribution-NonCommercial License (http://creativecommons.org/licenses/by-nc/4.0/), which permits unrestricted non-commercial use, distribution, and reproduction in any medium, provided the original work is properly cited. The terms on which this article has been published allow the posting of the Accepted Manuscript in a repository by the author(s) or with their consent.

domains into a bsAb. Finally, in vitro assembly of half-IgGs or monospecific IgGs (e.g., mosunetuzumab, amivantamab, epcoritamab, and teclistamab)[2] provides a flexible approach to the LC pairing problem, but as with cFAE, requires specialized expertise to express the antibodies in individual host cells and create bispecific end products.[2,14]

In this context, the relative advantages of manufacturing an IgG-like bsAb in a single host cell have been previously noted.[15–17] Analogous to the utility of Fc C_H3 (third constant domain of the heavy chain) KiH substitutions[2] for correct HC pairing, several efforts have been made to engineer Fab interfaces to enforce preferential LC pairing.[6] There are two large interchain domain interfaces within the Fab, variable light (V_L):variable heavy (V_H) and constant light (C_L):constant heavy first domain (C_H1), of roughly equal interface area, as well as two smaller intrachain interfaces: V_H:C_H1 and V_L:C_L. HC:LC pairing have been shown to be determined by the strength of the V_L:V_H interaction[18,19] and the cooperative stabilization[20–23] provided by the C_L:C_H1 interface, especially for Fabs with κ-germline LCs. This cooperativity makes it challenging to eliminate chain mispairing based on mutations in only one of the two primary inter-chain interfaces within the Fab[15,24,25]

The structural conservation of immunoglobulin domain interfaces[26] independent of variable domain sequence makes structure-based computational interface redesign of the native variable domains and wild-type (WT) constant domains to enforce correct LC pairing feasible. There are multiple reports on the structure-based computational design of orthogonal Fab interfaces. Lewis et al. [24] used the RosettaDesign protocol to design Fab heterodimerization substitutions and applied these primarily to bispecific antibodies containing a λ-germline LC in one or both Fab arms. Using a similar computational approach, Froning et al.[25] proposed a novel set of mutations for bispecific antibodies with the κ-germline LC isotype. Furthermore, Dillon et al.[15] used Rosetta calculations to design either hydrophobic-packing or charge-swap substitutions for bispecific antibodies with κ-germline LCs. Multiple IgG-like bispecific antibody constructs with redesigned Fab interfaces were experimentally characterized in these publications and exhibited near-complete elimination (<5%) of the mispaired LC chain species while maintaining the antigen-binding affinity and thermostability properties of their monospecific counterparts. However, these designs required AA substitutions within both the constant and variable domain interfaces to eliminate LC pairing, and designs with only redesigned constant domains exhibited significantly higher proportions of the mispaired species (typically >20%).[15]

As part of the overall derisking strategy in therapeutic antibody development, variable domain changes that could negatively impact antigen-binding affinity or developability should be avoided. From this viewpoint, LC pairing designs that involve AA substitutions only within constant domains are attractive[17,27–29] Such designs may theoretically be applied universally to arbitrary pairs of variable fragments (Fvs) to form IgG-like bispecifics without additional sequence modifications and have therefore been the subject of multiple recent literature reports. Mazor et al. [27] described the Duetmab technology that replaces the native C_H1:CL disulfide in one of the two Fab arms with an engineered disulfide to promote proper LC pairing in an EGFR × Her2 bsAb. Similarly, Golay et al.[28] incorporated charged and polar AA substitutions in the constant domains of one Fab arm of a CD5 × CD3 bsAb to prevent chain mispairing. Recently, Hikaru *et al.* [17] described a diverse panel of complementary C_H1:Cκ charged substitutions for the assembly of IgG-like bispecifics. They proposed that for bsAbs with relatively low levels of chain mispairing, particular designs with a total of eight AA substitutions across the two Fab arms may be sufficient. For higher levels of mispairing, additional constant domain mutations combined with a variable domain charge swap may be necessary to eliminate mispaired species.

Here, we present a computationally designed solution containing mutations only within the C_H1 and Cκ Fab constant domains to enforce the correct LC pairing in IgG-like bsAbs possessing κ-germline LCs on both Fab arms. Given the integral contribution of hydrogen bonds to the specificity of protein–protein interfaces,[30,31] we hypothesized that de novo design of non-native hydrogen bond interactions into the C_H1:Cκ interface could be used to create orthogonal sets of mutations with high predicted pairing specificity that could overcome the mispairing preferences of the variable domains. To efficiently search the large potential mutational space of all residues within the C_H1:Cκ interface, we applied the HBNet design algorithm[32,33] available in Rosetta to design novel hydrogen bonding networks. These HBNet designs were subsequently filtered using flex ddG[34] Rosetta calculations to select those with high predicted C_H1:Cκ specificity by maximizing the energy gap between the positive design (correctly paired) and negative design (mispaired) states, as well as the subunit interface stability. We incorporated these redesigned constant domain interfaces into an IgG-like bispecific format and experimentally characterized chain mispairing, antigen binding, and developability properties for multiple pairs of variable domains. These data converged onto a pair of complementary C_H1:Cκ interface redesigns (labeled 1443 and 1993) that led to the near-complete elimination of Fab mispairs, including in bsAbs with relatively high baseline levels of mispaired species in the context of WT Fab constant domains. These engineered bispecific IgG molecules also demonstrated high-expression titers in mammalian cell lines, favorable developability characteristics, and did not show increased immunogenic potential as assessed by an in vitro immunogenicity assay. Finally, the crystal structures of the mutant Fabs show that the 3D conformations of the complementarity-determining regions (CDRs) and domain interfaces remain similar to the original, with the presence of novel designed hydrogen bonds validating the Rosetta protocols used to introduce and score hydrogen bond interactions. Altogether, our computationally designed constant domain mutation sets present a broadly applicable method for bispecific antibody production, potentially advancing the efficiency and reliability of therapeutic antibody manufacturing.

Results

In silico design and characterization of single interface designs

Rosetta: HBNet design and flex ddG rescoring

We define a Single Interface Design (SID) four-chain bsAb as one that incorporates the WT C_H1:Ck domain interface on one

Fab arm and a mutated C_H1:Cκ domain interface on the other (illustrated in Figure 1). In contrast, a Double Interface Design (DID) bsAb is one with mutated C_H1:Cκ domain interfaces on both Fab arms. A SID has the advantage of potentially bearing fewer constant domain AA substitutions compared to DID bsAb, but mutations at both interfaces may be needed to fully overcome Fab mispairing. A SID requires the design of one novel C_H1:Cκ interface and the consideration of two mispaired states, making computations simpler compared to the design and evaluation of two novel interfaces and two mispaired states for a DID. For these reasons, we executed our study in two stages. In the first stage, we designed SIDs with the objectives of favorable interface stability and pairing preference, and experimentally characterized bsAbs containing these designs. We then built on these data to design DIDs in the second stage.

To generate SIDs, we used Rosetta's Monte Carlo HBNet hydrogen bond network design algorithm[32,33] on the WT C_H1 and Cκ domain coordinates from Protein Data Bank (PDB) ID 1fvd. We performed a two-sided design, permitting AA substitutions in both C_H1 and Cκ. The HBNet output contained a total of 3,571 C_H1:Cκ sequence pairs (Supplementary Figure S1) with 1,959 unique Cκ sequences, 1,657 unique C_H1 sequences, and a total of 3,164 unique C_H1:Cκ pairs (3,164/3,571 = 89% unique). Sequences with a minimum of one and a maximum of three AA substitutions per chain were retained to balance the potential energetic benefits of additional mutations while maintaining a native-like sequence. This reduced the number of unique C_H1:Cκ interfaces to 1,469.

Subsequently, we used the flex ddG protocol in Rosetta[34] to compute the scores for filtering and select designs for experimental characterization. The flex ddG protocol typically incorporates "backrub" protein backbone movements[35–37] that aid in more accurate modeling of the energetic effects of mutations than a fixed backbone context.

The stability and the cognate pairing preference of each SID were assessed by computing the differences in binding energy after mutation between the HBNet-derived designs and reference interface states. For interface stability, we used the WT C_H1:Cκ interface as the reference and for pairing preference we used two SID mispairs: mutated C_H1 paired with WT Cκ and mutated Cκ paired with WT C_H1. The ideal C_H1:Cκ design is one that is more stable than the WT C_H1:Cκ and also more stable than either mispaired state. We defined the comparison of the positive, correctly paired design state to the mispaired states as the Rosetta Heterodimerization Score (RHS, see Materials and Methods). In each comparison, we considered the total Rosetta energy and the hydrogen bond component of the score function separately, leading to four energy filters for a given C_H1:Cκ design. To minimize computational costs at this stage, flex ddG assessments were made without incorporating backrub-generated backbone flexibility. The context of alternate starting WT conformations was assessed by running flex ddG simulations on each of four WT C_H1:Cκ PDB templates (1aj7, 1l7i, 4olv, and 6b14) and averaging the resulting energies.

We observed that 265/1,469 designed interfaces had more favorable (more negative) total Rosetta interface energies compared to the WT, and 991/1,469 had more favorable hydrogen bond interface energies. Similarly, 283/1,469 designs returned better total Rosetta interface energies compared to the average of the mispaired states, or 1,092/1,469 when considering only the hydrogen bond component of the score function. The high fraction of unfavorable designs as scored by flex ddG Rosetta energies suggeststhat many HBNet-designed residue interactions were incompatible with their surrounding environment. In summary, a set of 172/1,469 designs passed all four energy filters and were retained at this filtering step.

Next, we performed Rosetta energy calculations within the flex ddG protocol and utilized backrub-generated backbone flexibility to obtain better modeling accuracy. This computationally intensive step was restricted to a set of 84/172 novel designs representing a diverse set of mutated position combinations and AA substitutions. Filtering was applied to carry forward each designed C_H1 and Cκ sequence only once, in combination with the opposite-chain sequence predicted to be most energetically compatible. Several designs that appeared to have overpacked charged residues, identified upon visual inspection, were also eliminated during this selection process. Twenty of the resulting best scoring designs were selected based primarily on their RHS for experimental testing in SID bsAbs. The scores of the correctly paired and mispaired states for the best five of these 20 selected designs are shown in Figure 1. An accounting of the number of designs that passed each filtering step of the computation design and selection pipeline is given in detail in Supplementary Table S1.

To minimize the mutational load in the designs, reversions to the WT AA residue at the substituted positions were evaluated computationally prior to experimental production. For each design, an exhaustive scoring of all possible single and multiple substitution reversions (leaving at least one substitution in each chain) was performed using the flex ddG protocol. When the impact of the best set of reversions on the cognate pairing preference was predicted to be minimal (≤1 Rosetta energy unit change, see Materials and Methods), the design with reversions was carried forward. Energies for the eight designs in which reversions passed filters are shown in Supplementary Figure S2. To ensure that designs chosen for experimental characterization sampled a diverse set of mutated positions, their locations in structural space were examined. Structural analysis confirmed that the 20 sequences selected for experimental characterization covered diverse positions on the C_H1:Cκ interface (Supplementary Figure S3).

In summary, we computationally created a novel set of 20 C_H1:Cκ SIDs that mutated a diverse set of interface positions, were predicted not to be destabilizing, and were predicted to favor correct pairing when expressed in competition with WT C_H1:Cκ sequences.

Experimental characterization of single interface designs

Next, we chose the variable regions of the therapeutic antibodies panitumumab (anti-EGFR) and ustekinumab (anti-IL-12/IL-23) to characterize mutation sets in a bispecific IgG format. All bispecific antibody productions were done using a plasmid ratio of 1:1:1:1 for the two HC and two LC chains. Four-chain

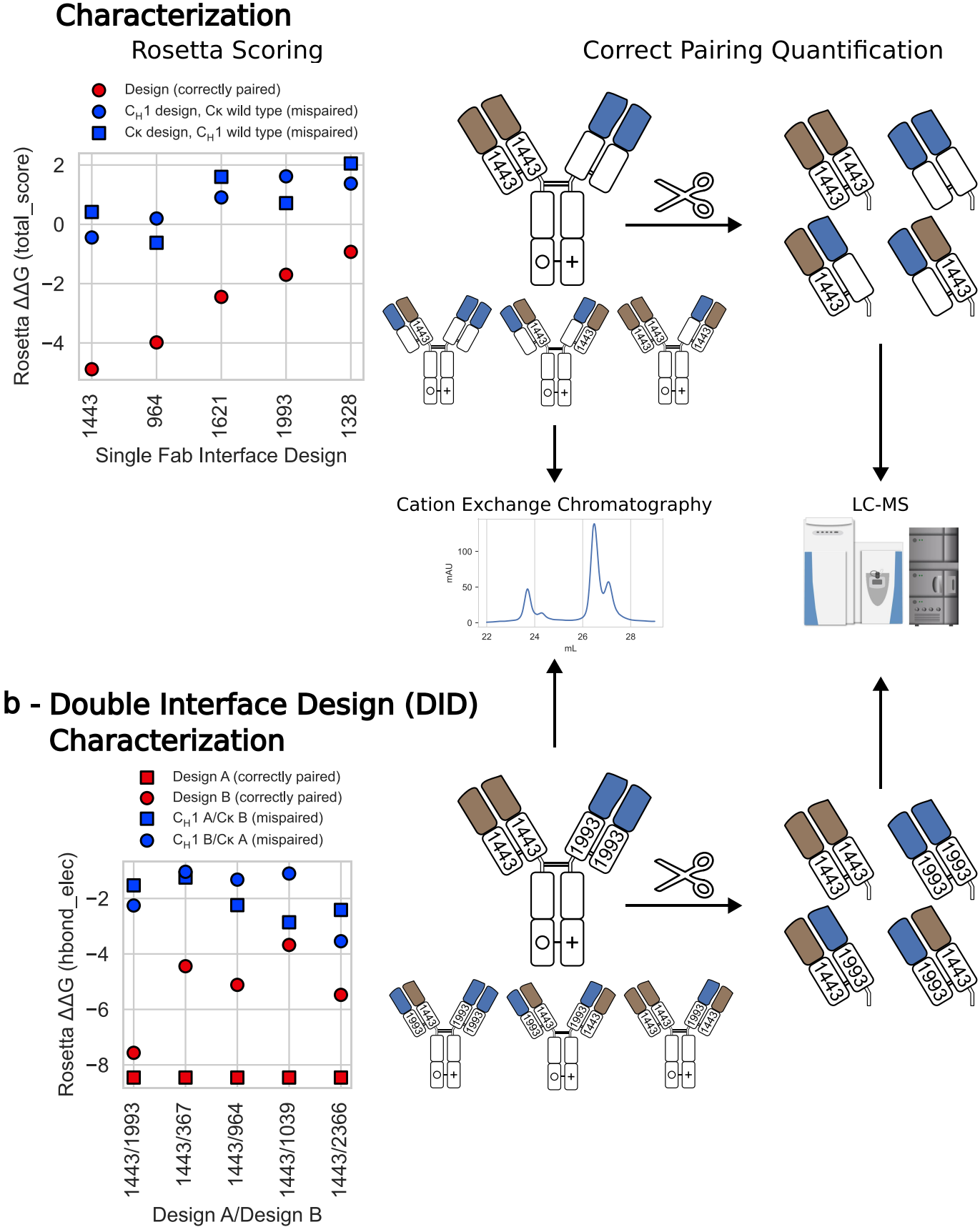

Figure 1. Schematic summarizing the design and experimental process followed to obtain novel heavy chain/light chain constant domain pairing mutation sets. (a) Rosetta flex ddG scores (after 18,000 backrub steps) of the top five best single Fab interface designs (SIDs), representing the initial in silico scoring step. Larger predicted energetic gaps between the positive design state (red circle) and negative design states (blue circles) indicate a prediction of stronger ability to enforce correct pairing. The right side of the schematic depicts the experimental workflow used to quantify pairing. Panitumumab and ustekinumab variable domains are shaded brown and

transfections of panitumumab and ustekinumab with WT heavy and light chain constant domains produced high titers of mispaired-chain species, indicating low cognate HC:LC pairing preference within the two variable domains and a robust challenge for pairing mutations to overcome (data not shown). C_H1:Cκ mutations were installed in the constant regions of the panitumumab arm, along with the knob mutation in the ustekinumab arm C_H3 (T366W), hole mutations in the panitumumab arm C_H3 (T366S, L368A, and Y407V) and an engineered disulfide (knob: S354C; hole: Y349C) to enforce correct heavy-chain pairing[38–40]

Data were obtained for 18 of the 20 produced samples across two independent HEK-293 transient productions, with two samples dropped due to an inability to differentiate species via liquid chromatography-mass spectrometry (LC-MS) or due to a low production titer (Table 1). The IgGs were digested into Fabs for LC-MS quantification to improve LC-MS resolution and to focus on the heavy chain-light chain pairing separately from heavy-chain heterodimerization (see Materials and Methods)[41,42] We reference individual sets of designed C_H1:Cκ interface mutations via their serial identifier output by the HBNet design algorithm (e.g., design 1443 or design 1993). Overall, eight of 18 samples showed equivalent or higher correct pairing proportions than WT, as measured by LC-MS of IgGs digested into Fab material. The percentage of correctly paired-chain species was 79% for the WT, i.e., without any constant domain mutations. Designs 1039 and 1443 returned the largest increases with the percentage of correctly paired species at 88% and 86%, respectively. Size-exclusion chromatography (SEC) main peak quantification remained >90% for all but two tested designs (Table 1). Process yields, which are expected to be highly variable in HEK-293 transient transfections, showed a general but moderate decline from the yield observed for the WT sample. Four designs were included in both productions and exhibited similar correct pairing percentages in both (as well as a later third production, Supplementary Table S2), indicating that the LC-MS quantification of chain pairing was reproducible across independent experiments.

Computational predictions of correct pairing, using various flex ddG protocol options, were compared to experimental results to benchmark the effectiveness of the in silico scoring protocol. As shown in Supplementary Figure S4, using only the hydrogen bond and electrostatic components of the Rosetta energy function, and 18,000 backrub sampling steps, returned a better rank correlation (Spearman ρ=-0.78) with Fab LC-MS-measured correct pairing than flex ddG scoring with zero backrub steps, or using the total Rosetta score. This indicates that both the hydrogen bond and charge interactions are likely major mechanistic drivers of the correct pairing and confirms that incorporating backbone flexibility improves interface $\Delta\Delta G$ predictions.

In conclusion, eight of our 18 experimentally tested C_H1:Cκ SIDs drove equivalent or higher correct pairing than a WT C_H1:Cκ control, validating our computational design pipeline and allowing us to next apply the computational protocol to select the best combinations of designs.

DID pairing production/characterization

Although bsAbs containing computationally designed SIDs displayed improved correct pairing rates over WT controls, these designs did not achieve our desired goal of 100% correct pairing. To reach this goal, we tested IgGs containing designed C_H1:Cκ interfaces on both Fab arms in the DID context.

Experimentally tested SIDs with a low production titer (≤75 mg/L), poor LC-MS-measured correct pairing, and/or poor SEC were not carried forward. Remaining SIDs were computationally screened in a pairwise matrix of DID combinations of C_H1 and Cκ domains using the Rosetta flex ddG protocol. Based on an earlier comparison of the correct pairing predictions to experimental SID results (Supplementary Figure S4), the hydrogen bond and electrostatic score-term components of the Rosetta energy function, with 18,000 backrub sampling steps in the flex ddG protocol, were used to rank-order the designs. While the best scoring SIDs had a maximum predicted Rosetta heterodimerization score of about −4 Rosetta energy units, the best scoring DID combinations now had scores < −6, indicating a stronger prediction of correct pairing (Suplementary Table S3).

To reduce the number of required cloning steps, two designs that were frequently members of the best scoring combinations of designs – designs 1443 and 1039 – were chosen to function as design "A" (one of the two C_H1:Cκ designed sets of mutations present in a DID) in the context of ustekinumab variable domain sequences. These two designs were screened against five designs (design "B") each, which were cloned in the context of panitumumab variable domain sequences. Rosetta scoring of the top 10 DID sequences is shown in Figure 1(b). The largest Rosetta Heterodimerization Score energetic gap of about −6 Rosetta energy units was observed for DID 1443/1993, predicting that this design combination would be most likely to enforce correct pairing independently of variable domain context.

These 10 designs were produced via HEK-293 transient transfection (Table 2). All 10 tested DIDs returned a higher percentage of correctly paired species relative to the matched WT bsAb baseline of 71%. Four of the design combinations had 95% or higher correctly paired species, with one combination, 1443/1993, not showing any detectable mispairing via LC-MS. The intact bispecific IgG samples were also assayed

blue, respectively. IgG-like bispecifics that incorporate the top-scoring Rosetta designs in one of the Fab arms, and C_H3 knob-into-hole mutations for heavy-chain heterodimerization, were expressed in HEK-293 cells. Correct pairing was then assayed via two experimental methods: cation exchange chromatography on intact IgGs, and LC-MS quantification on IgGs digested into Fabs. (b) Rosetta flex ddG scores for double interface design's (DIDs) that contain mutation sets installed in both Fab arms of the IgG-like bispecific.

Table 1. Experimental characterization of single interface designs (SIDs). Columns list the analytic SEC main peak quantification after production, the process yield of the transient transfection production process, and the LC-MS observed percentage of Fabs containing each possible C_H1:Cκ combination, as well as the sum of correctly paired species. Designs are identified by a unique numeric identifier and ordered by the descending level of correct pairing. EU numbering is used for mutated C_H1 and Cκ positions.

					LC-MS observed Fab C_H1/Cκ				
Design	C_H1 Mutations	Cκ Mutations	SEC Main Peak %	Process Yield (mg/L)	Design/Design	Design/WT	WT/Design	WT/WT	Total Correct Pairing
WT	N/A	N/A	95.3%	369	37%	9%	12%	42%	79%
1039	H168S, V185S, T187D	L135R	95.8%	195	32%	12%	0%	56%	88%
1443	L145Q, K147E, S181E	T129R, T178R, T180Q	96.5%	200	35%	7%	7%	50%	86%
742	K147N, V185Y	T129R, T180S	94.9%	274	33%	9%	10%	48%	81%
2529	K147T, V185Q	L135S, T178R	97.2%	173	28%	18%	2%	53%	81%
367	D148R	Q124S, T129E	93.3%	91	36%	8%	12%	44%	80%
1993	L128R, K147R	Q124E, V133Q, T178E	94.1%	261	34%	6%	14%	46%	80%
1328	G166K, T187K	N137S, N138E	89.8%	192	33%	6%	15%	46%	79%
1888	T139R, A141Q, T187Q	S114D, L135S, N138R	93.3%	137	33%	9%	12%	46%	79%
1621	L145S, K147N	V133Y, T180R	96.3%	289	37%	7%	15%	41%	78%
2366	H168R, V185E	L135S	95.3%	180	33%	11%	11%	45%	78%
767	K147H, D148E	S127R, T129R	95.4%	146	35%	10%	14%	41%	76%
964	S124R, K147R	S127D, T129E	94.9%	274	36%	12%	12%	40%	76%
838	G166K, T187K	S114Q, N137T, N138E	89.2%	298	23%	6%	21%	50%	73%
384	L145S, S181Q	V133Y	92.1%	175	32%	9%	19%	40%	72%
394	K147R, Q175E, S181Q	T129D, T180Q	93.0%	234	31%	6%	21%	41%	72%
1148	L145S	V133Y	93.6%	200	34%	10%	18%	38%	72%
454	L145S	Q124E, V133Y	95.0%	244	36%	11%	18%	35%	71%
1048	L145Q, S181E	P120S,T178H, T180Q	97.9%	52	21%	24%	10%	45%	66%

Table 2. Experimental characterization of double interface designs (DIDs). Columns list the analytic SEC purity after ProA capture, the process yield of the transient transfection production process, and the LC-MS observed percentage of Fabs containing each possible C_H1:Cκ combination (correctly or incorrectly paired), as well as the sum of correctly paired species. Design A and Design B constant domain mutations were installed in the ustekinumab and panitumumab Fab arms, respectively.

				LC-MS observed Fab C_H1/Cκ designs				
Design A	Design B	SEC Main Peak %	Process Yield (mg/L)	A/A	A/B	B/A	B/B	Total Correct Pairing
WT	WT	94.6	231	30%	21%	8%	41%	71%
WT	1443	95.9	172	45%	8%	8%	39%	84%
WT	1039	96.0	165	50%	0%	10%	40%	90%
1443	1993	97.6	160	47%	0%	0%	53%	100%
1039	1993	86.3	131	38%	3%	0%	59%	97%
1443	964	98.1	140	36%	3%	2%	59%	95%
1443	1039	96.2	113	45%	0%	5%	50%	95%
1443	367	97.6	136	42%	0%	6%	52%	94%
1443	2366	97.2	147	42%	2%	4%	49%	91%
1039	367	91.1	107	28%	13%	0%	59%	87%
1039	2529	91.3	85	38%	0%	21%	41%	79%
1039	742	94.7	84	27%	15%	0%	49%	76%
1039	2366	90.0	109	36%	5%	22%	37%	73%
1443	WT	98.0	149	38%	4%	4%	54%	92%
1039	WT	92.9	123	24%	18%	3%	55%	79%

via cation exchange chromatography (CEX) as an orthogonal method to measure correct pairing (Supplementary Table S4). Quantification of the main observed peak in this assay was not expected to reach 100%, due in part to the effects of various charge variants. DID 1443/1993 returned the highest proportion of correctly paired species with 88% CEX main peak. CEX purity correlated well with LC-MS correct pairing (Spearman $\rho = 0.77$, Supplementary Figure S5), validating the use of LC-MS to measure correct pairing percentages to select the final design lead. As an additional check of the correct pairing, dual antigen binding to EGFR and IL-12B, the respective targets of panitumumab and ustekinumab were confirmed via a bridging assay in which bispecific molecules were captured with one antigen and then assessed for binding to the second (Supplementary Figure S6).

Notably, the design predicted to have the largest energetic gap by Rosetta between correctly paired and mispaired states, 1443/1993, is the same design that showed the best correct pairing experimentally. The 1443 design includes three C_H1 AA substitutions (L145Q, K147E, and S181E) and three Cκ substitutions (T129R, T178R, and T180Q), while the 1993 design includes two C_H1 substitutions (L128R, K147R) and three Cκ substitutions (Q124E, V133Q, and T178E), overall comprising 11 substitutions at eight unique C_H1 and Cκ residues. Of these mutations, 8/11 are substitutions for charged residues (E, R, and K), and

the remaining three substitutions are to Gln (Q). Our Rosetta scoring process to select designs again correlated well with LC-MS quantification of correctly formed heterodimers (Supplementary Figure S7), with the total score now showing the best correlation ($\rho = -0.89$), and the hydrogen bond plus electrostatic score components the second best (ρ=-0.80), both representing values obtained after 18,000 backrub steps in the flex ddG protocol.

We compared the ability of DID 1443/1993 to drive correct pairing against previously published solutions for IgG heavy/light chain pairing.[15,25] While these solutions incorporate AA substitutions in both the variable and constant domains, we tested only the respective constant-domain substitutions to directly compare against the constant domain mutations of DID 1443/1993. To evaluate the correct pairing under challenging conditions, we assembled monospecific IgGs with the panitumumab variable domains in both Fab arms, each paired with distinct orthogonal constant domain substitutions. Because both Fab arms contain identical variable domains, any pairing pressure had to originate from constant domain mutations. Correct pairing was quantified after digestion of IgG material into Fabs and quantification via LC-MS (Supplementary Table S5). DID 1443/1993 exhibited 98% correct pairing, significantly outperforming the two referenced literature mutation sets, which yielded 56% and 74% correct pairing.

An initial developability assessment for the 10 bispecific antibodies was performed using two high-throughput assays that have previously demonstrated utility in predicting desirable downstream clinical properties[43]: hydrophobic interaction chromatography (HIC) and an assessment of polyspecificity (also referred to as polyreactivity) using a polyspecificity reagent (PSR).[43,44] Polyspecificity is a highly undesired property that has been linked to poor antibody pharmacokinetics[45,46] and HIC column retention time can be used to screen for soluble molecules with desired low hydrophobicities. Measured HIC retention time remained unaffected after the introduction of constant domain mutations, with no discernible change compared to WT, and all values were within the previously defined low hydrophobicity range of retention times (≤10.5 min)[43] (Supplementary Figure S8a). In addition, the PSR values remained in the "no polyreactivity" score range (≤0.1)[45] (Supplementary Figure S8b).

To summarize, we computationally designed combinations of C_H1:Cκ SIDs that were predicted to strongly favor correct pairing. Experimental testing revealed that one combination comprising designs 1443 and 1993, showed no measurable mispaired HC:LC via LC-MS and retained the preexisting desired biophysical properties. When tested in a difficult monospecific format, DID 1443/1993 drove 98% correct pairing, substantially outperforming previously reported constant domain-only mutation sets, which required the addition of variable region mutations to achieve high levels of correct pairing in their tested contexts.

Validation of the top DID in additional variable domain contexts

We next tested the generalizability of DID 1443/1993 to achieve correct-chain pairing via a larger panel of bispecifics with a new set of antibody variable regions. Variable regions of four additional human antibodies, ofatumumab, fresolimumab, necitumumab, and sifalimumab (targeting CD20, TGFβ, EGFR, and IFN-α, respectively), were chosen to test as bispecifics along with panitumumab and ustekinumab. Collectively, these represent a diverse set of V_H and Vκ germlines and were chosen to include challenging combinations with low propensities to correctly pair, based on previous assessments (data not shown). Molecular weight was also considered so that the bispecific pairs of variable regions would possess large enough differences to make LC-MS quantification of correct pairing possible. Five bispecific combinations of the six variable regions were selected and produced in HEK-293 cells as IgGs: ofatumumab/sifalimumab, fresolimumab/necitumumab, necitumumab/sifalimumab, and fresolimumab/ofatumumab, along with the originally tested pairing of panitumumab/ustekinumab.

In addition to bispecific combinations of these variable regions with mutation sets 1443 and 1993, we created monospecific controls containing the same variable region on both Fab arms of the IgG. These two-chain controls solely contained designed mutation sets 1443 or 1993 in both Fab arms along with WT C_H3 domains. With these constructs, the impact of the designed mutations on the physiochemical developability properties of IgGs could be studied without the added complication of sample heterogeneity due to chain mispairing.

All variable region combinations were produced as IgGs and digested into Fabs to assess correct pairing proportions by LC-MS (Figure 2a). All five bispecific combinations showed nearly 100% LC-MS correct pairing in at least one of the two possible orientations (e.g., mutation set 1443 on the panitumumab arm, and 1993 on the ustekinumab arm in one combination, or 1443 on the ustekinumab arm and 1993 on the panitumumab arm in the other), and no mispaired species were observed for two of the five tested bispecifics. Strikingly, although the baseline pairing propensities of the five tested combinations of variable regions (with unmodified constant regions) varied widely from 54% to 80%, DID 1443/1993 was able to enforce correct pairing to nearly 100% in all cases. The most difficult pair of variable regions to combine into a bispecific, necitumumab and sifalimumab (which showed 54% correct pairing with WT C_H1:Cκ) did not show mispairing via Fab LC-MS when combined into a bispecific with DID 1443/1993, albeit with reduced titers compared to WT (yield around 90 mg/L, compared to 257 mg/L for WT C_H1:Cκ).

As an orthogonal measurement, we assessed IgG correct pairing by CEX for panitumumab and ustekinumab bi- and monospecifics (Figure 2b). Main-peak quantification of panitumumab × ustekinumab bispecific samples shows correct pairing approaching the levels quantified in the monospecific controls, indicating that little or no mispairing occurred.

In summary, installing constant region mutation sets 1443 and 1993 on each Fab arm of an IgG drove near 100% correct pairing in all tested bispecifics produced in HEK-293 cells.

Developability assessment of CHO-produced bispecfics

We next produced a panel of five bsAbs in a Chinese hamster ovary (CHO) cell line to produce additional material for

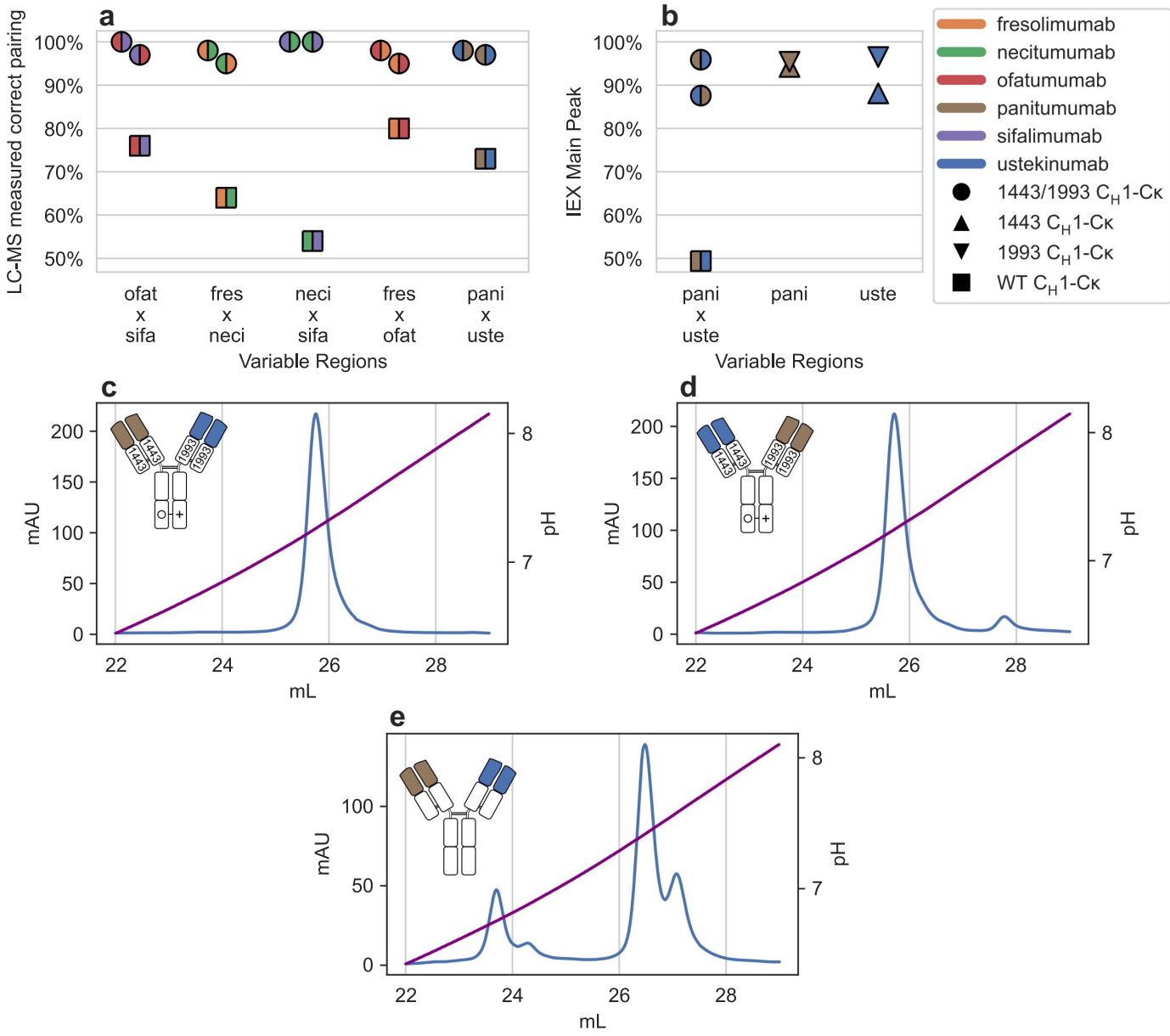

Figure 2. (a) Correct pairing in multiple variable region contexts, as measured by LC-MS quantification of Fab material digested from HEK-293-produced IgGs. Variable domains are assigned colors (shown in legend). Wild-type bispecific controls, with no C_H1:Cκ mutations, are depicted as squares. Data for DID bispecifics produced with the 1443 and 1993 designs are depicted as circles. The different split colorings for the circles represent alternate combinations of variable regions and constant domain mutation sets. (b) CEX main peak quantification of intact IgG-like bispecific containing variable domains from panitumumab and ustekinumab. Monospecific control samples arising from 2-chain transfections, with the same 1443 or 1993 set of mutations on both Fab arms, are depicted as triangles. (c) Representative CEX traces of panitumumab/ustekinumab bispecific IgG sample produced with corresponding constant region mutation sets 1443/1993, and Hole/Knob C_H3 mutations, along with an antibody schematic illustrating the domain sequences in the intended, correctly paired bispecific sample. Main peak quantification of this trace (96%) is represented as the circular point with the highest main peak quantification in panel (b). (d) CEX traces of the alternative variable domain/constant domain pairing shown in panel (c), with a C_H1:Cκ constant domain containing mutation set 1443 linked with an ustekinumab variable domain, and mutation set 1993 with panitumumab. Main peak quantification of this trace (88%) is also depicted in panel (b). (e) Reference CEX trace of a control produced with wild-type C_H1:Cκ domain sequences and wild-type C_H3 domains, with a main peak quantification of 49%. The antibody schematic represents the corresponding bispecific IgG with correctly paired heavy and light chains.

characterization and to test production in a mammalian cell host commonly used for manufacturing therapeutic antibodies.[47] We also produced monospecific controls to study the potential developability risks of mutation sets 1443/1993 individually in the context of multiple variable domains. As previously, proteins were purified on a protein A column without further polishing, and both LC-MS and CEX were used to quantify correct pairing.

The LC-MS assessment of the CHO-produced bispecifics showed near-complete elimination of chain mispairing, replicating the results of the earlier HEK-293 production (Supplementary Figure S9). LC-MS and CEX measurements of the correct pairing continued to correlate well (Supplementary Figure 10), although a switch to a higher-resolution analytical CEX instrument added more variability to the main peak quantifications.

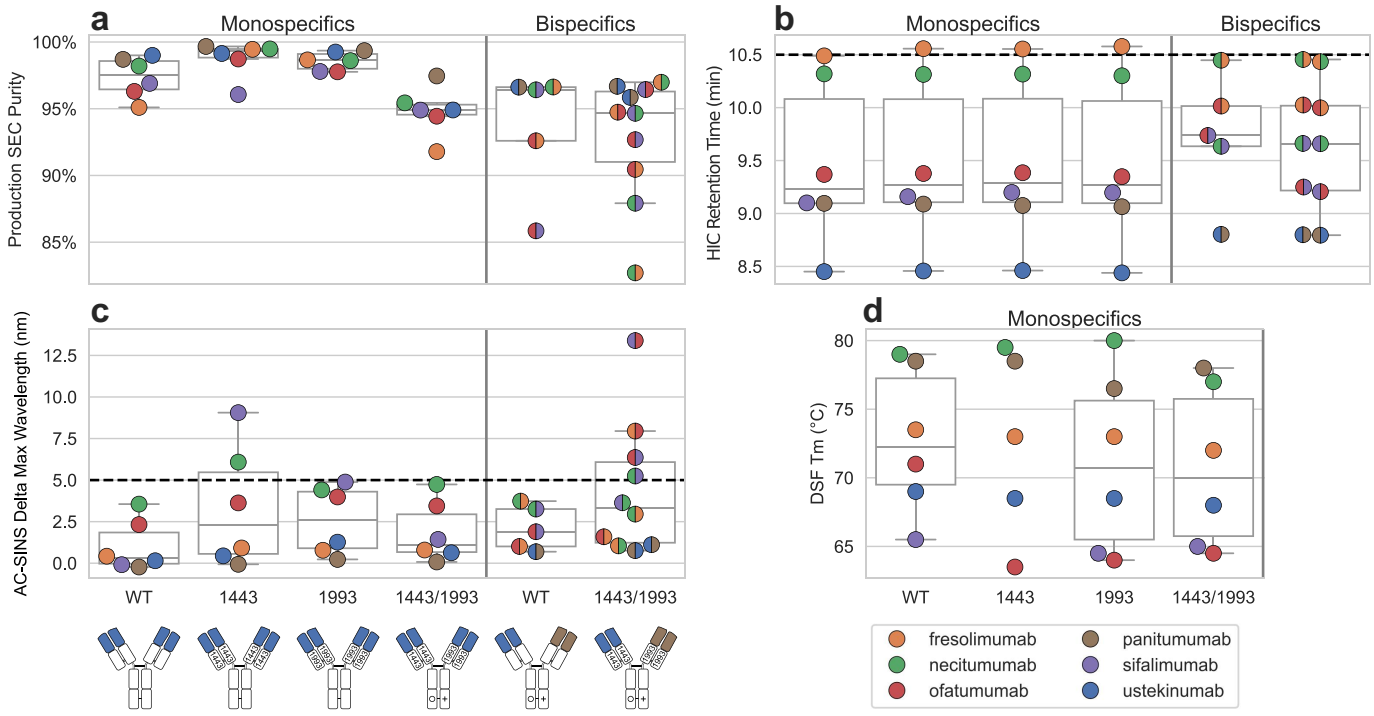

Figure 3. Summary of high-throughput biophysical and developability characterization data. Variable domains are assigned colors (shown in legend). Monospecific IgGs containing one set of variable domain sequence are shown as solid colored circles. Bispecifics, consisting of unique variable domains, are shown as split circles, with each half of the circle indicating one of two paired variable domains present in the molecule. Most bispecific combinations of variable domains are present twice, indicating that they were produced in two separate orientations with 1443/1993 (e.g., 1443 paired with variable domain a in one point, or 1443 paired with variable domain B in the other). A schematic of example constructs is shown below panel C. (a) Size exclusion chromatography (SEC) purity, as measured by main peak percentage. (b) Hydrophobic interaction chromatography (HIC) column retention time. (c) Affinity-capture self-interaction nanoparticle spectroscopy (AC-SINS) (d) Fab T_m, as measured via differential scanning fluorimetry (DSF) assay. No boxplot is shown for monospecific T_m values for design 1443 due to lack of available data for sifalimumab.

For each monospecific control (identical variable regions in each Fab arm) and bispecific IgGs, purities were further assessed by SEC (Figure 3a). Monospecific controls with WT constant domains or with Fab arms containing only one of the 1443 or 1993 mutation sets (and C_H3 KiH), typically return SEC purities >97%. DID monospecific controls containing the 1443 mutation set in one Fab arm, and the 1993 mutation set in the other show a slight reduction in SEC purity, down to a median of 95%. For each of the bispecific IgGs, there was at least one orientation that returned an SEC purity >95%. For panitumumab × ustekinumab bispecific, SEC purity was high (96 or 97%) in either orientation of variable domains and designed mutations (1443 or 1993). In contrast, for the necitumumab × fresolimumab bispecific, one orientation yielded a high SEC purity (97%), while the reverse orientation yielded 83% purity.

Further developability assessments revealed that HIC retention times were unaffected by the introduction of 1443 or 1993 pairing mutations, with HIC values for bispecific antibodies observed to correspond to the average of their two constituent monospecific values, regardless of whether C_H1:Cκ was mutated or not (Figure 3b).

The panel of monospecifics and bispecifics was also assessed for changes in their self-association propensities via the Affinity-capture self-interaction nanoparticle spectroscopy (AC-SINS) assay.[48] The presence of mutation sets 1443 or 1993 slightly increased AC-SINS on average (Figure 3c), although the average across the panel of variable domains remained below the previously described threshold of 5 nm that was found to be associated with clinical progression.[48] As with SEC purity, the orientation of variable regions with constant region mutation set matters, as bispecific molecules showed varying AC-SINS values depending on their orientation.

Additionally, the stability of the Fab domains was assessed via differential scanning fluorimetry (DSF), which showed a small decrease in Fab melting temperatures (T_m) for some monospecific IgGs containing constant domain mutations (Figure 3d). This decrease was much smaller than the variation in T_m associated with variable region identity. Stability was also studied via assay of the temperature at the onset of aggregation, T_{agg}, which was studied for a subset of bispecific samples. For the panitumumab × ustekinumab and necitumumab × sifalimumab bispecifics, T_{agg} remained similar to WT in one orientation of 1443/1993, while it was reduced in the reverse orientation (Supplementary Table S6). However, in the context of fresolimumab and ofatumumab, T_{agg} was reduced in both orientations of constant domain design sets. While no systematic trends were observed, this result again points to the potential benefits of screening multiple orientations as part of the bispecific development process of a specific pair of variable domains to flag developability issues.

Introduction of design sets 1443 or 1993 reduced the total yield of bispecific samples produced via transient expression in CHO cells, from 212 mg/L for bispecific samples produced with WT C_H1:Cκ constant regions, to 185 mg/L for samples

produced with DID 1443/1993 (Supplementary Figure S11a). However, a higher proportion of correctly paired bispecific materials should at least partly compensate for any decrease in yield caused by constant domain mutations, especially as their effect in the context of larger-scale stable cell-line productions is yet to be studied.

Finally, the other studied properties of polyspecificity (investigated via PSR binding assay, Supplementary Figure S11b) and stability after pH 3.5 stress (a condition that mimics the low pH viral inactivation hold step in manufacturing, Supplementary Table S7) did not show any systematic negative effects attributable to the introduction of the designed 1443 and 1993 C_H1:Cκ mutation sets. No oxidation, deamidation, or isomerization of residues in the C_H1:Cκ constant regions was observed post-low-pH stress in samples containing mutation sets 1443 or 1993 (data not shown). No significant effect on antigen binding for monospecific IgGs containing mutation sets 1443 or 1993 was observed compared to WT by Biacore binding kinetics measurements (Supplementary Figure S12), although further experiments in the context of bispecifics with both designed mutation sets may be warranted to verify maintenance of binding after the simultaneous introduction of both pairing mutation sets.

In summary, the 1443 or 1993 constant domain mutation sets did not induce any large systemic negative effects on developability across the tested panel of variable domains. As some metrics, such as SEC purity, AC-SINS, T_m and T_{agg} showed variation in certain orientations of variable domain and constant domain mutation sets, standard screening assays should still be applied to study and select for molecules with the most favorable developability properties.

In vitro assessment of immunogenicity risk

The presence of mutations in the constant domains of bispecific antibodies may introduce additional risks for immunogenicity and the elicitation of anti-drug antibody (ADA) responses.[49] Although a comprehensive assessment of a protein's immunogenicity is only possible through clinical trials, in vitro approaches can be used to assess a protein's immunogenic potential prior to clinical evaluation.[50] To assess the immunogenic risks associated with the 1443/1993 mutation sets, we adapted a previously published in vitro T cell activation assay. This assay is based on the reported correlation between the expression of two T cell co-stimulatory receptors (CD134 and CD137) in $CD4^+$ T cell populations following co-culture with biotherapeutic and ADA rates elicited by that therapeutic in clinical trials.[51]

To validate this assay, we cultured peripheral blood mononuclear cells (PBMCs) from 20 hLA-typed donors with the known immunogen keyhole limpet hemocyanin (KLH). As donor HLA alleles shape the epitopes presented to surveilling $CD4^+$ T cells and therefore the immune responses to biotherapeutics,[50] the donor cohort was selected for diverse HLA-DR allele representation, with allele frequencies that are representative of North American populations (Figure 4a, Supplementary Table S8).[52] Following either 2 or 7 days of co-culture, stimulation index (SI) values were calculated by comparison to donor-matched medium-only controls (Supplementary Figure S13), as previously described.[49] Donor SI values were significantly ($p < 0.01$) higher at day 7 and 16/20 (80%) donors exhibited a positive response (SI ≥ 2) to the KLH at this timepoint (Figure 4b), supporting the use of these conditions in subsequent co-culture experiments.

We next sought to validate this assay's ability to correctly identify biotherapeutics with high potential for immunogenicity. To this end, we selected nine control IgGs with either low (bevacizumab, palivizumab, and secukinumab), intermediate (adalimumab and ixekizumab), or high (AMG 317, ATR-107, bococizumab, and HuA33) clinical incidences of ADAs for evaluation. Except for palivizumab, each of these IGGs has been previously evaluated using similar in vitro assays.[49,53] Consistent with their clinical immunogenicity, three of the four high ADA IgGs elicited positive responses in 50–65% of the donors (Figure 4c). In contrast, only a single positive donor response was observed for one of the five low- and intermediate-ADA controls. These results suggest that this in vitro assay can stratify biotherapeutics based on their immunogenicity risk.

To assess the impact of 1443/1993 constant domain pairing mutation sets on the immunogenic potential of engineered antibodies, we next evaluated monospecific and bispecific IgGs encoding these mutation sets in the context of the variable domains of palivizumab and/or bevacizumab. These variable domains were selected because unmodified palivizumab and bevacizumab did not elicit immunogenic responses in our initial screenings (Figure 4c). Donor responses were evaluated against either unmodified palivizumab, monospecific palivizumab modified on both Fab arms with either the 1443 or 1993 mutation sets (containing WT C_H3 domains) or a palivizumab × bevacizumab bispecific IgG containing 1443 (palivizumab arm) and 1993 (bevacizumab arm) mutations and a set of internally developed KiH C_H3 domain mutations for heavy-chain heterodimerization (see Materials and Methods). Notably, none of the five samples elicited a positive response from the 20 donor samples despite robust responses to the positive control KLH in 18/20 (90%) donors, suggesting that the 1443/1993 pairing mutation sets do not increase the immunogenic potential of these antibodies (Figure 4d).

Finally, we reassessed each IgG with a novel optimized protocol to ensure that sub-optimal assay read-outs had not obscured small changes in immunogenicity attributable to the 1443 or 1993 mutation sets. We modified our assay for the quantification of inducible costimulatory molecule (ICOS) expression, which showed significantly enhanced ($p = 0.029$) SI values relative to CD134 and CD134 following 7 days of co-culture with KLH, with 20/20 (100%) donors exhibiting a positive response at this timepoint (Figure 4b). Re-evaluating the panel of nine clinically controlled IgGs with this optimized metric, we found that all four high-ADA control IgGs now elicited a positive response in 10–65% of the donors, while four of the five low- and intermediate-ADA controls elicited donor responses in one or fewer donors (Figure 4e). However, even with this optimized metric, we did not observe any positive donor responses to monospecific IgGs containing 1443 or 1993 mutation sets, and only one (5%)

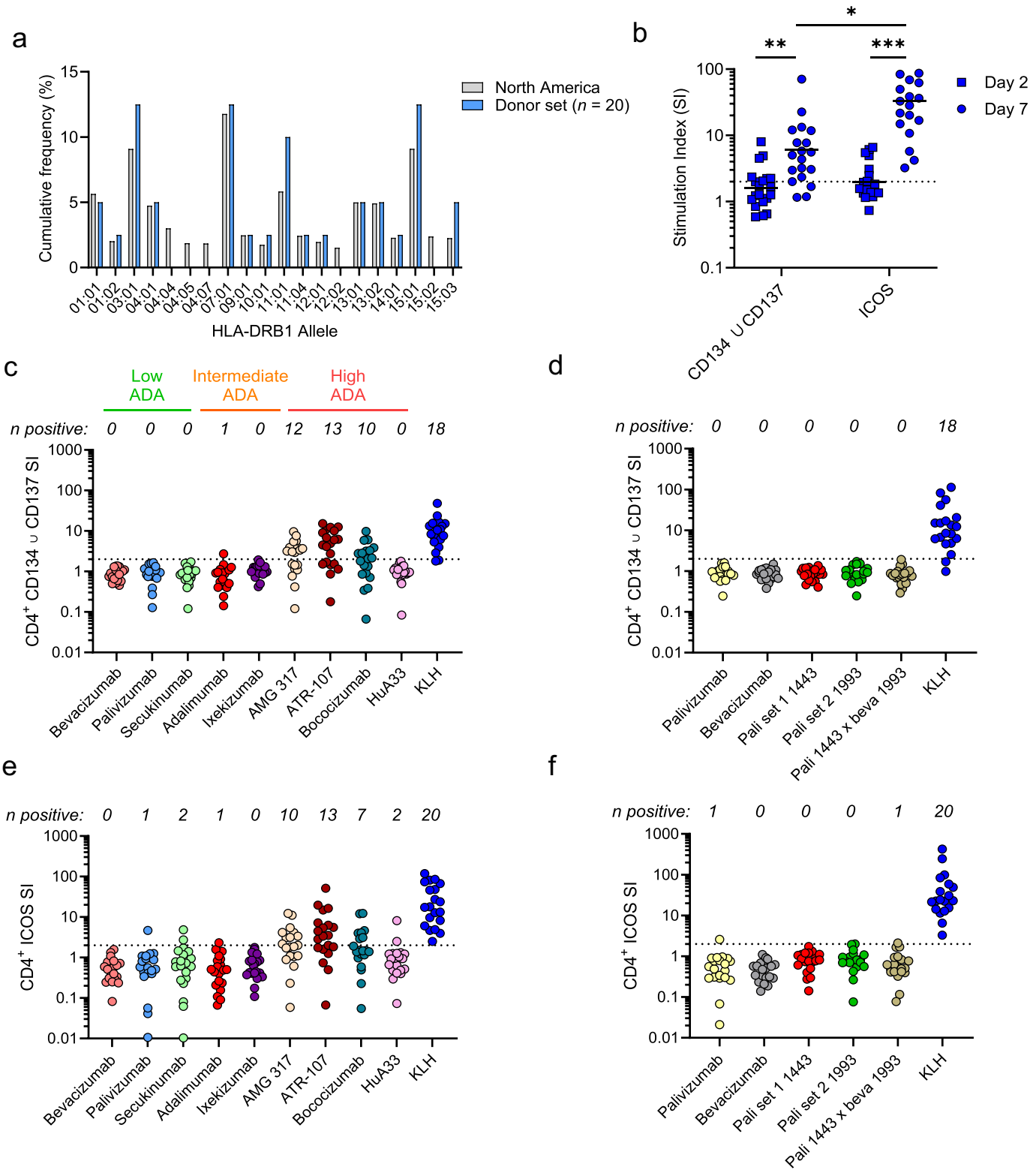

Figure 4. 1443/1993 antibody pairing mutation sets do not confer additional risks for immunogenicity. a) Frequency of the top 20 most prevalent HLA-DR alleles among North American populations, averaged across gold-standard datasets on allelefrequencies.Net, and among the PBMC donor cohort selected for in vitro T cell stimulation assessments. b) Calculated stimulation index (SI) values for enrichment of CD134 and CD137 (CD134 ∪ CD137) or ICOS expression in CD4+ T cell populations following 2 or 7 days of co-culture with KLH, as assessed by flow cytometry. Statistical comparisons calculated by two-sided Friedman's tests with Dunn's correction for multiple comparisons. *, $p < 0.05$; **, $p < 0.01$; ***, $p < 0.001$. c,d) Calculated CD134 ∪ CD137 SI values among CD4+ T cells following 7 days of co-culture with either monospecific control IgGs with known clinical anti-drug antibody (ADA) response rates (c) or monospecific and bispecific IgGs based on palivizumab and bevacizumab bearing 1443 or 1993 antibody pairing mutation sets, alongside wild-type IgG controls (d). e,f) Calculated ICOS SI values among CD4+ T cells following 7 days of co-culture with either monospecific control IgGs with known clinical ADA response rates (e) or monospecific and bispecific IgGs based on palivizumab and bevacizumab bearing 1443 or 1993 antibody pairing mutation sets, alongside wild-type IgG controls (f).

donor exhibited a positive response to the palivizumab × bevacizumab bispecific IgG, further supporting the low immunogenicity risks of these constant region mutations (Figure 4f).

In summary, our in vitro assessment of mAbs bearing 1443/1993 constant domain mutation sets did not find evidence that these mutations conferred additional risks of immunogenicity.

Crystal structures and structural analysis

To understand the structural basis for the Fab pairing specificity achieved by the computational designs, we obtained crystal structures of Fabs containing the variable regions from panitumumab and the 1443 (PDB ID: 9MFN) or 1993 (PDB ID: 9MI7) mutation sets (Figure 5). The Fab structure for design 1443 was fit to a final R and R_{free} of 20.8% and 22.1%, respectively (electron density shown in Supplementary Figure S14). The Fab structure for design 1993 was built with a final R and R_{free} of 18.0% and 23.0% (density shown in Supplementary Figure S15). Large structural rearrangements in the C_H1:Cκ were not observed, with a backbone root mean squared deviation in these regions to WT panitumumab structure 5SX4[54] of 0.45 Å in the 1443 structure and 0.43 Å in the 1993 structure. Nine of the eleven mutated residues are almost completely buried in the C_H1:Cκ domain interface (fractional burial >75%), while two positions (design 1443; LC: 129R and 180Q) are partially exposed to solvent (fractional solvent-accessible surface area burial 40–60%). All six mutated residue side chains in the structure of design 1443 (Figure 5a) were well connected with hydrogen bonds, including inter-chain salt bridges between mutated residues HC 147E and LC 129R, and HC 181E and LC 178R (EU numbering). The structure of design 1993 shows one hydrogen bond involving mutated residue side chains across the C_H1:Cκ interface between HC 128R and LC 131S. Thus, the designed network of electrostatic and H-bond interactions arises primarily from contributions in the buried core of the C_H1:Cκ domain interface. When superimposed on each other (Supplementary Figure S16), the structures of design 1443 and design 1993 show several inter-chain steric overlaps, indicating that mispairing may not be possible without structural rearrangement that is likely to be energetically infeasible.

We investigated the similarity of starting HBNet models and flex ddG models generated with or without backrub-generated backbone flexibility to their corresponding crystal structures to determine which Rosetta-generated models most closely matched the structures. For design 1993, mutant side chains in flex ddG models match the crystal structure of rotamer bins more frequently (54% rotamer bin match) than the starting HBNet model (20% rotamer bin match, Supplementary Figure S17). For design 1443, correct rotamer matching is not significantly improved by backbone sampling and remains low for both flex ddG-generated models (18%) and the original HBNet model (17%). Alignments of the Rosetta models with the lowest Local Distance Difference Test for the crystal structures are shown in Supplementary Figure S18. As the flex ddG models used to rank designs do not, in general, contain the same rotamers present in the crystal structures of the resulting designs, the improved performance of flex ddG in ranking designs when utilizing backbone flexibility may result from better scoring of mispaired states. In addition, the average score of the ensemble of generated flex ddG models may still be a better predictor of correct pairing, even if no individual model in the ensemble correctly captures all mutated side-chain rotamers observed in the low-energy crystal structure state.

Discussion

The 2024 installment of the "Antibodies to watch" series lists 20 clinical-stage bispecific antibodies;[55] 50% of these are formatted as IgG-like molecules using a diverse set of enabling chain-pairing technologies.[55] This snapshot, as well as the regulatory approvals issued for multiple IgG-like bispecifics (db.antibodysociety.org), underscores the continued interest in the development of antibody engineering solutions for correct heavy chain/light chain assembly for bispecifics.

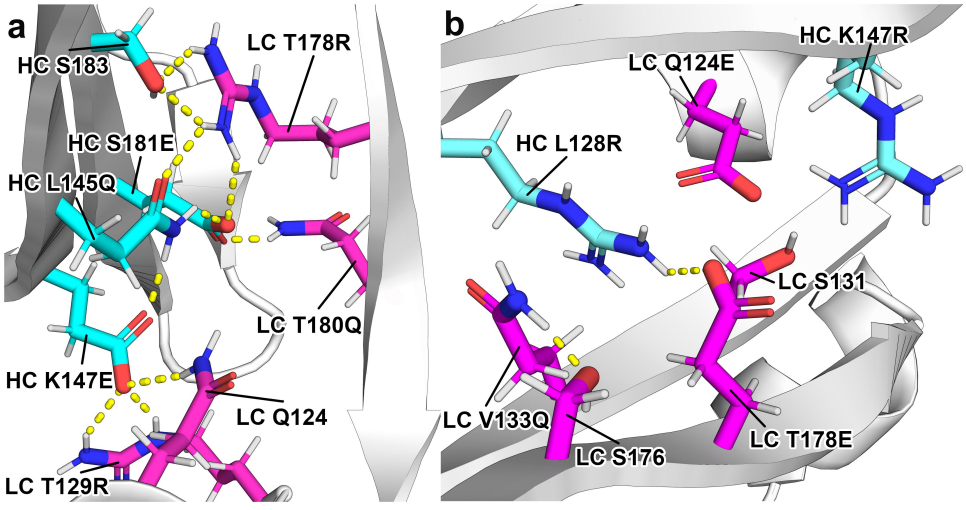

Figure 5. (a) Crystal structure of design 1443. (b) Crystal structure of network 1993. Hydrogen bonds (bonds and hydrogen atom placement determined in Rosetta via H-bond feature analyzer) are shown in both panels. Mutated side chains, or residues with side chains involved in hydrogen bonds with mutated residue side chains, are shown as sticks.

The 1443 and 1993 computationally designed orthogonal mutation sets were tested using a panel of five bsAbs incorporating a diverse set of six cognate HC:LC variable domain pairs to measure LC mispairing rates in four-chain IgG-like bispecifics. We demonstrated that the combined 1443 and 1993 DID leads to near-complete (≥98% correct pairing in at least one variable/constant domain orientation) elimination of HC:LC mispairing in all cases, including notably for the necitumumab × sifalimumab bsAb that returns only 54% correct pairing without the designed mutations. Beyond the case studies presented here, the 1443/1993 mutation set has also been installed in a panel of CD20/CD3 bispecific molecules which show activity in a redirected T cell cytotoxicity assay.[56] Further testing of these mutation sets in the context of variable domains with even greater propensities to mispair natively will be helpful in determining how universally these constant domain-only mutations can enforce correct pairing.

While the computational design of buried polar or H-bond interactions at protein–protein interfaces has proven to be challenging in the past,[57,58] there are examples of computational design of polar or hydrogen-bond interaction networks at natural or *de novo* designed protein interfaces[30,31,33,59,60] An early example was the Rosetta-based design of a *de novo* hydrogen bond network at the DNase-immunity natural protein interface that resulted in a 300-fold specificity switch relative to the cognate interaction.[30] More recently, HBNet design protocols were used to design H-bond networks in the context of *de novo* designed coiled-coil homo- and hetero-oligomers.[33,59,60] Our work builds on these examples and highlights the ability of the HBnet design sampling approach to introduce new ionic and H-bond interactions into the natural C_H1:Cκ interface that is dominated by hydrophobic interactions.[61]

Notably, not all intended designed hydrogen bonds that appeared in the original HBNet model structures are observed in the Fab crystal structures of the designs. This fact, along with the proximity and high number of charge mutations introduced, points to charge-based pairing preference as a potential major driving mechanism of the mutations. Flex ddG-derived models show better rotamer recovery, highlighting the key role this scoring played in the design process, including being the only scoring step in which negative state energies of mispaired states were considered.

Some prior examples of Rosetta-based bispecific design explicitly considered multiple states simultaneously during sequence design by optimizing against negative design states (mispaired heavy and light chains) in parallel with the design of a stable positive state (correctly paired chains).[24,25] Here, HBnet-based sampling generated a sufficient number of novel, stable, and correctly paired interfaces such that subsequent flex ddG screening could find combinations against WT interfaces, and other HBNet-derived designs, with large enough energetic penalties to enforce correct pairing.

FDA-approved IgG-like bispecific antibodies have been observed to have a relatively low level of immunogenicity in clinical trials[62–64] despite the associated protein engineering and manufacturing technologies incorporated into these molecules. However, there are published reports of adverse clinical immunogenicity of bsAbs attributed to factors, such as novel B-cell and T-cell epitopes in the engineered variable domains,[63,65,66] or non-IgG-like molecular formats,[67] so care should be taken to verify that the constant region mutations that enable bsAb formation do not introduce novel immunogenicity risk. Importantly, our in vitro T cell activation assay results in this study did not show increased risks of immunogenicity due to the introduction of the 1443 or 1993 designed mutation sets. However, the additional regulatory scrutiny[68] invited by bispecifics may justify additional studies to further validate these findings.

Altogether, we present a computationally designed set of constant domain-only mutations that can enforce correct heavy chain/light chain pairing in multiple tested variable domain contexts in single-cell hosts, which suggests value in producing correctly assembled bispecific material in the context of downstream manufacturing and production. High throughput screening assays did not show generally increased downstream developability risks, and an in vitro immunogenicity assay similarly did not show increased risk of immunogenicity. Crystal structures of the 1443 and 1993 mutation sets revealed the presence of several novel hydrogen bonds introduced by the designs. The computational design process of hydrogen bond network design, followed by multi-state rescoring with sampled backbone flexibility, serves as a template to create other preferentially paired protein–protein interfaces.

Materials and methods

Rosetta and computational design process

Rosetta version r188 (2018.33 + release.7111c54) was used for HBNet, and r215 (2019.12 + release.46f270e) was used for flex ddG scoring. Flex ddG scores were created as previously described,[34] with the Talaris2014 score function specified in the Rosetta script and used by invoking Rosetta with the "-restore_talaris_behavior" flag. Hydrogen bond and salt bridge statistics were output by the hydrogen bond feature reporter,[69,70] and these Rosetta-assigned hydrogen bonds were the source of hydrogen bonds annotated in figures.

We define the RHS used to evaluate the predicted strength of mutations to enforce correct pairing as the difference of change of binding energy after mutation between the desired correctly paired states and the average change of binding energy of the mispaired states.

Change in binding energy from Rosetta's flex ddG algorithm is defined as:

$$\Delta\Delta G_{bind} = \Delta G_{bind}^{MUT} - \Delta G_{bind}^{WT}$$

Rosetta Heterodimerization Score is defined for SIDs as:

$$RHS = \Delta\Delta G_{bind}^{Correctly\ paired\ state} - \Delta\Delta G_{bind}^{Mispaired\ state}$$

Rosetta Heterodimerization Score is defined for DIDs as:

$$RHS = \Delta\Delta G_{bind}^{Correctly\ paired\ state} - \frac{\Delta\Delta G_{bind}^{Mispaired\ state\ 1} + \Delta\Delta G_{bind}^{Mispaired\ state2}}{2}$$

As previously described, flex ddG scores are calculated as described above for individual Rosetta trajectories, and the results averaged over multiple independent trajectory runs.

For each of the 20 designs selected for experimental characterization, an exhaustive scoring of all possible single and multiple substitution reversions (leaving at least one substitution on each chain) was performed using the flex ddG protocol with no backrub flexibility. The best scoring set of substitutions to revert (lowest scoring set of WT reversions by total score RHS) was then evaluated using the flex ddG protocol with backrub-generated backbone flexibility. If the resulting total score of RHS increased by ≤1 REU, and the hydrogen bond RHS score increased by ≤0.5 REU, then the reversion set of substitutions was chosen to be carried forward.

Cloning and mammalian production

Synthetic double-stranded gene fragments (Integrated DNA Technologies™) encoding V_H, V_L, and designed C_H1 and Cκ domains were amplified and subcloned into pcDNA™3.4+ vectors (ThermoFisher, Catalog no. A14697) by NEBuilder® HiFi DNA assembly (New England Biolabs®, Catalog no. E2621). The HC vectors encoded a WT IgG1 C_H2 domain and either a Knob or Hole C_H3 domain. Assembly reactions were transformed into 5-alpha F'*Iq* Competent *E. coli* (New England Biolabs®, Catalog no. C2992). Transformants were screened by PCR and Sanger sequencing to identify clones with the desired HC and LC sequences. Plasmids were isolated from positive colonies using NucleoBond® Xtra Midi Endotoxin-free plasmid DNA purification kits (Macherey-Nagel Inc., Catalog no. 740420). DNA concentrations were obtained by measuring A260 on Nanodrop™. The plasmid DNA sequence was confirmed by Sanger sequencing for final verification.

BsAbs were expressed transiently in either HEK293 or CHO-S cells grown in shake flasks. After 6 or 9 days of production, respectively, the cell culture supernatant was harvested by centrifugation and passed over Protein A resin (MabSelect SuRe™ from Cytiva). The bound antibodies were then washed with phosphate-buffered saline (PBS) and eluted with a buffer consisting of 200 mm acetic acid and 50 mm NaCl at pH3.5 into 1/10th volume 2 M HEPES, pH 9.0. The yields were determined by measuring the protein concentration using A280 NanoDrop™.

SEC

The mammalian production and protein A purification products were further analyzed for purity (as determined by the percentage of monomer full-size antibodies among all antibody products) by SEC. An Agilent 1260 hPLC (Agilent, Santa Clara, CA) with a TSKgel Super SW mAb HTP column (TOSOH Bioscience, King of Prussia, PA) was equilibrated with 200 mm sodium phosphate, 250 mm sodium chloride pH 6.8 at a flow rate of 0.400 mL/min. Approximately 2–5 µg of protein sample was injected onto the column and monitored at 280 nm. Total assay time was approximately 6 min. Data was analyzed using ChemStation software.

PSR

Polyspecificity of each bsAb was measured as described previously.[45] Briefly, soluble membrane protein (SMP) and soluble cytosolic protein (SCP) fractions obtained from CHO cells were biotinylated using NHS-LC-Biotin (Thermo Fisher Scientific Cat#21336). IgGs presented on the surface of yeast[71–73] were incubated with 1:10 diluted biotinylated CHO cell preparations on ice for 20 min. Cells were then washed twice with ice-cold PBS containing 0.1% bovine serum albumin (BSA) (PBSF) and incubated in 50 µL of a secondary labeling mix containing ExtrAvidin-R-PE (Sigma-Aldrich), anti-human LC-FITC (Southern Biotech) and propidium iodide for 15 min. The cells were washed twice with PBSF and resuspended in PBSF to be run on a FACSCanto II (BD Biosciences). The mean fluorescence intensity of binding was normalized using control antibodies that display low, medium, or high polyspecificity to assess the nonspecific binding. Antibodies were rated as clean (PSR score < 0.11), low (0.11 < PSR score < 0.33), medium (0.33 < PSR score < 0.66), and high polyspecificity (PSR score > 0.66).

HIC

HIC was performed to assess hydrophobic interaction of the lead antibodies. The methodology for this assay was described previously.[74] In brief, 5 µg IgG samples (1 mg/mL) were spiked in with a mobile phase A solution (1.8 M ammonium sulfate and 0.1 M sodium phosphate at pH 6.5) to achieve a final ammonium sulfate concentration of about 1 M before analysis. A Sepax Proteomix HIC butyl-NP5 column was used with a liner gradient of mobile phase A and mobile phase B solution (0.1 M sodium phosphate, pH 6.5) over 20 min at a flow rate of 1 mL/min with UV absorbance monitoring at 280 nm. Hydrophobicity levels were determined based on the retention time of the chromatographic analysis. Hydrophobicity flag ranges are defined as: clean to low when the retention time is <10.5 min; medium when the retention time is ≥10.5 and <11.5 min; and high when the retention time is ≥11.5 min.

Dual binding

All experiments were performed at 25°C on a ForteBio Octet HTX instrument (Sartorius, Göttingen, Germany). All reagents were formulated into PBS with 0.1% (w/w) BSA (PBSF). Monomeric human EGFR-moFc (100 nM) was first loaded to anti-mouse Fc IgG capture sensor tips (Sartorius, Göttingen, Germany) and then allowed to stand in PBSF for a minimum of 15 min. These loaded sensor tips were initially exposed (60 s) to wells containing PBSF to establish a stable baseline for the assay before exposure (180 s) to the bispecific IgG (100 nM) and then finally (600 s) to human IL-12 (100 nM). Bispecific IgGs with sufficient binding responses in the final two steps of the assay were classified as dual binders.

LC-MS

Bispecific antibodies were analyzed for pairing using LC-MS. IgG Samples were first subjected to GingisKHAN® (Genovis,

Inc.) digestion to obtain Fab fragments, and the digest was then split into two aliquots. One aliquot was directly analyzed by LC-MS for correct HC-LC pairing, and the other was reduced by dithiothreitol before LC-MS measurement (data not shown). Briefly, samples were injected onto an Acquity Ultra Performance liquid chromatography (UPLC) system (Waters), equipped with a Thermo Scientific MabPac RP® 4 µm column (2.1 × 100 mm) maintained at 80°C. After injection, samples were eluted from the column using a 13-min gradient from 20% to 55% acetonitrile at a flow rate of 0.3 mL/min (mobile phase A: 0.1% formic acid in LC-MS grade H_2O; mobile phase B: 0.1% formic acid in LC-MS grade acetonitrile). Species eluted from the column were detected by a Q Exactive mass spectrometer (Thermo Scientific) in positive electrospray ionization mode. The instrument parameters were set as a spray voltage of 3.5 kV, capillary temperature of 350°C, sheath gas flow rate at 35 and aux gas flow rate at 10 and S-lens RF level at 90. MS spectra were acquired in the scan range of 750–4000 m/z. Acquired MS data were analyzed using Biopharma Finder software (Thermo Scientific) followed by manual inspection to ensure correct assignment and relative quantification accuracy. Relative quantitation for each of the pairs and pair species was calculated based on the intensities of the peaks with respect to the sum of all the pairs and pair peak intensities.

Confirmation of correct pairing trends by CEX

CEX chromatographic separations were performed on a computer-controlled ÄKTA™ Avant 150 preparative chromatography system equipped with an integrated pH electrode, enabling in-line pH monitoring, and a Mono S 5/50 GL column. The cation exchange buffer was composed of 15.6 mm CAPS, 9.4 mm CHES, 4.6 mm TAPS, 9.9 mm HEPPSO, 8.7 mm MOPSO, 11.0 mm MES,13.0 mm Acetate, 9.9 mm Formate, 10 mm NaCl, and the pH was adjusted up to 4.0 (buffer A) or 11.0 (buffer B) using NaOH. 500 µg of protein was buffer exchanged into 25% buffer B and filtered through a 0.2 µm filter. Before each separation, the column was equilibrated with 10 column volumes of 25% buffer B. The protein was then loaded onto the column via a capillary loop, followed by a 10 column volume wash with 25% buffer B, a 20 column volume linear pH gradient from 25% to 100% buffer B, and a 10 column volume hold at 100% buffer B.

aCEX

Analytical CEX was performed on an Agilent 1260 Infinity II HPLC with a ProPac WCX-10 hPLC column (Thermo Fisher Scientific). The cation exchange buffers were the same as described in the section above. The column was equilibrated in 80% Buffer A. Five µgs of sample were injected and separated with a linear gradient from 80% to 0% Buffer A over 23 min at a flow rate of 0.35 mL/min and a column temperature of 30°C. The column was re-equilibrated for 10 min in 80% Buffer A before the next sample injection. Samples were analyzed with the Agilent OpenLab CDS Software. Sample retention time drift was monitored using a bracketing control antibody.

Fab T_m

The melting temperature (T_m) of monospecific antibody samples was measured by differential scanning fluorometry (DSF). Twenty microliters of the sample, at 0.1–1 mg/mL, was mixed with 10 µL of 20× Sypro orange (Sigma-Aldrich) before being subjected to a controlled temperature increase from 40°C to 95°C, at 0.5°C intervals in a C1000 thermocycler (Biorad) to collect fluorescence signals. Melting temperatures were obtained by taking the negative of first derivative of the raw signal.

Aggregation temperature

Tagg for antibodies produced in CHO cells was measured as follows: 8.8 µL of sample was loaded in duplicate to 16 × 9 µL micro cuvettes (Unchained Labs, Norton, MA); three of the 16 × 9 µL micro cuvettes were loaded at a time into Uncle (Unchained Labs, Norton, MA); T_{agg} 266 with optional DLS was selected as the application with a temperature range of 15°C to 95°C; intrinsic fluorescence measurements and static light scattering measurements at 266 nm and 473 nm were taken for each sample replicate at 1°C intervals; the data was subjected to analysis using Uncle Analysis V5.03 software (Unchained Labs, Norton, MA) to determine T_{agg} 266.

pH3.5 stress by SEC

Antibodies produced in CHO cells were analyzed for tolerance to low pH by SEC. Samples at 20 mg/mL were buffer exchanged into PBS (200 mm phosphate buffered with 250 mm sodium chloride, pH 7.0) and pH 3.5 buffer (50 mm sodium chloride, 200 mm acetic acid, pH 3.5). After 1 h at room temperature (25°C), buffer exchanged samples were diluted to 1 mg/mL in PBS (200 mm phosphate buffered with 250 mm sodium chloride, pH 7.0), and 2 µg of sample was injected into an Agilent 1260 Infinity analytical HPLC (Agilent, Santa Clara, CA) fitted with a TSKgel SuperSW mAb HTP column (TOSOH Bioscience, King of Prussia, PA). SEC data was collected and subjected to analysis using the Agilent ChemStation software.

Surface plasmon resonance kinetics

Surface plasmon resonance kinetic analysis was conducted at 25°C in an HBS-EP+ running buffer system (10 mm HEPES pH 7.4, 150 mm NaCl, 3 mm EDTA, 0.05% Surfactant P20) using a Biacore 8K optical biosensor (Cytiva USA, Marlborough, MA) docked with a CM5 sensor chip. Goat anti-human IgG capture antibody (109-005-098, Jackson ImmunoResearch Laboratories, Inc., West Grove, PA) was immobilized (~8000 RU) to both flow cells of the sensor chip using standard amine coupling chemistry. This surface type provided a format for reproducibly capturing fresh analysis antibody after each regeneration step. The sample compartment was maintained at 10°C for the duration of each experiment. All other samples and reagents were formulated into a running buffer. Each experiment cycle began with an injection (10 s at 10 µL/min) over flow cell 2 of antibody (5.0 nM).

This was followed by an injection of (180 s at 30.0 μL/min) of a series of antigen concentrations (180–0.25 nM) over flow cells 1 and 2. The dissociation of the antibody/antigen complex was monitored for 600 s. Several blank buffer samples were injected (180 s at 30 μL/min) over flow cells 1 and 2 and used for reference surface subtraction. Finally, three injections (30 s at 30 μL/min) of regeneration solution (10 mm glycine, pH 1.7) over flow cells 1 and 2 prepared the sensor surface for another cycle. For data processing and fitting, the sensorgrams were cropped to include only the association and dissociation steps. This cropped data was subsequently aligned, double reference subtracted, and then non-linear least squares fit to a 1:1 binding model using Biacore Insight Evaluation software version 3.0.11.15423.

Affinity-capture self-interaction nanoparticle spectroscopy

The AC-SINS assay was performed as described previously.[48,75] In short, gold nanoparticles (15705; Ted Pella Inc.) were coated with goat anti-human Fc-specific IgG (109-005-098; Jackson ImmunoResearch). The antibodies of interest were then incubated with the particles for 1 h and the wavelength shift was measured using Molecular Devices SpectraMax M2 with SoftMax Pro6 software. Self-interacting clones show a higher wavelength shift away from the PBS sample.

T cell stimulation assays

Cryopreserved, HLA-typed human PBMCs were purchased from Immunospot (Catalog no. CTL-HP1). Cryotubes containing >10^7 PBMCs were thawed in a 37°C water bath and resuspended in an AIM-V medium (Gibco™, Catalog no. 12055-083) supplemented with 5% CTS™ Immune Cell SR (Gibco™, Catalog no. A2596101) and 1% penicillin-streptomycin (Gibco™, Catalog no. 15140122). Thawed PBMCs were pelleted at 4°C for 10 min at 500 × g, washed twice, and cultured in a 24-well plate in 1 mL media at a density of 2.0×10^6 cells/ml. PBMCs were cultured either in media only, with 50 μg of test IgG, or with 100 μg of KLH (Sigma-Aldrich, CAS Number: 9013-72-3, SKU: H7017-50 MG). Following incubation at 37°C with 5% CO_2 for either 2 or 7 days, cells were washed twice with ice-cold fluorescence-activated cell sorting (FACS) buffer [Dulbecco's PBS (DPBS; VWR, Catalog no. L0119–1000) supplemented with 2% fetal bovine serum and 1 mm EDTA (Invitrogen Catalog no. AM9262)] and stained with 100 μL of FACS buffer containing anti-human 1:100 CD19 (PerCP-Cy5.5; Biolegend Catalog no. 302230, RRID:AB_2073119), 1:100 CD14 (PerCP-Cy5.5; Invitrogen, Catalog no. 45-0149-42, RRID:AB_1518736), 1:100 CD16 (PerCP-Cy5.5; Biolegend, Catalog no. 360712, RRID: AB_2562955), 1:100 CD56 (PerCP-Cy5.5; Biolegend, Catalog no. 318322, RRID:AB_893389), 1:100 CD4 (PE-Cy7; Biolegend, Catalog no. 357410, RRID:AB_2565661), 1:100 CD3 (APC; Biolegend, Catalog no. 300412, RRID: AB_2562045), 1:100 CD134 (BV510; BD, Catalog no. 745040, RRID:AB_2742665), 1:100 CD137 (BV711; Biolegend, Catalog no. 309832, RRID:AB_2650990), 1:100 ICOS (PE; Biolegend, Catalog no. 313508, RRID:AB_416332), and 1:500 propidium iodide (PI; Sigma-Aldrich, catalog no. P4170) for 20 min on ice. Cells were then washed twice, resuspended in ice-cold FACS buffer, and analyzed on a BD FACS Aria II Fusion (BD Biosciences). For each sample, data for 10,000 live $CD4^+$ T cells ($PI^-CD19^-CD14^-CD16^-CD56^-CD4^+$) were collected and analyzed for their expression of CD134, CD137, and ICOS surface markers using FlowJo v10.9 (FlowJo, LLC). Stimulation index (SI) values were calculated as previously described. Briefly, CD134 ∪ CD137 SI values were calculated by dividing the cumulative proportion of $CD134^+$, $CD137^+$, and $CD134^+CD137^+$ cells among live $CD4^+$ T cells by the matched proportion in the donor-matched medium-only control. ICOS SI values were calculated correspondingly.

Antibody samples for T cell stimulation assays

Clinical-grade bevacizumab (Avastin), palivizumab (Synagis), secukinumab (Cosentyx), adalimumab (Humira), ixekizumab (Taltz), and evolocumab (Repatha) IgGs were purchased from Evidentic GmbH. AMG 317, ATR-107, bococizumab, HuA33 IgGs, and monospecific palivizumab IgGs containing 1443 or 1993 mutations were produced in CHO cells. Published antibody VH or VL sequences were cloned into either WT, 1443 mutant, or 1993 mutant human IgG1-isotype heavy-chain or kappa light-chain expression vectors, respectively. IgGs were then expressed in CHO cells by transient transfection, purified by protein A (ProA) affinity chromatography, and polished to at least 95% purity by ceramic hydroxyapatite chromatography. Plasmids for the expression of the bispecific palivizumab (1443 mutant) × bevacizumab (1993 mutant) IgG were designed similarly, with the addition of T366W S354C (palivizumab arm) and T366S Y407G Y349C (bevacizumab arm) knob-into-hole CH3 domain mutations for heterodimerization. Bispecific IgG was produced in CHO cells via 4-chain transfection followed by ProA purification and was polished to >99% purity by ion-exchange chromatography. All samples contained less than 1 EU/mg of endotoxin as assessed by LAL (limulus amebocyte lysate) assays.

Crystallization and structure determination of Fab containing 1443 mutation set

A human Fab, referred to as ADI-64596 and comprising panitumumab variable domains along with the design mutation set 1443 C_H1 (of IgG1) domain comprising L145Q, K147E, and S181E substitutions and a Cκ domain comprising T129R, T178R, and T180Q substitutions, was concentrated to 11.35 mg/mL into a buffer containing 2 mm Tris-HCl pH 8.0 and 150 mm NaCl. The PACT, BCS, and JCSG+ screens (all from Molecular Dimensions Ltd.) were initially set up using a mosquito crystallization robot (STP Labtech). Since crystals obtained from these initial screens only gave rise to low-resolution X-ray diffraction, crystal seed solutions were prepared and applied in the setup of the BCS, PACT, and Additive Screens (Hampton Research). Sitting drops of 160 nL protein and 160 nL precipitant solution were left to equilibrate against a 40 μL reservoir at 20°C. After a few days, plate and needlelike crystals appeared in several conditions. The

precipitant solution giving rise to the best-diffracting crystal contained 75 mm Tris pH 8.5, 25 mm Bis-Tris-propane pH 8.5, 22.5% (v/v) PEG Smear Low, 5% (w/v) PEG3350, 50 mm NaBr. The crystal was flash-cooled in liquid nitrogen after soaking in precipitant solution supplemented with 10% (v/v) PEG400 as cryo-protectant. Data were collected at the synchrotron beamline I04, Diamond Light Source, UK, at 100 K and λ = 0.9795 Å. 3600 images were collected with an oscillation range of 0.1° per image. The beamline is equipped with a Dectris Eiger2 XE 16 M detector. Data extending to 2.35 Å were processed using XDS[76] Aimless[77] and reindexed to correspond with the data set of the Fab containing the 1993 mutation using the Sftools software of the CCP4i suite.[78] Crystals consisted of a single molecule in the asymmetric unit (ASU) in $P3_1$ space group. A molecular replacement solution for the Fab was obtained by PHASER[79] using the crystal structure of the panitumumab WT C_H1:Cκ Fab.[54] The structures were built manually in COOT[80] and refined using PHENIX[81] to a final to a final R and R_{free} of 20.8% and 22.1%, respectively. Coordinates and structure factors have been deposited in the PDB under the accession code 9MFN.

Crystallization and structure determination of Fab containing 1993 mutation set

A human Fab, referred to as ADI-64597 and comprising panitumumab variable domains along the design mutation set 1993 C_H1 (of IgG1) domain comprising L128R and K147R substitutions and a Cκ domain comprising Q124E, V133Q, and T178E substitutions was concentrated to 16.5 mg/mL into a buffer containing 2 mm Tris-HCl pH 8.0 and 150 mm NaCl. PACT, BCS, and JCSG+ screens (all from Molecular Dimensions Ltd.) were set up using a mosquito crystallization robot (STP Labtech). Sitting drops of 150 nL protein and 150 nL reservoir solution were left to equilibrate against a 40 µL reservoir at 20°C. After a few days, needlelike crystals were obtained in several conditions. The crystal used for data collection was obtained in the BCS screen, condition B10 (0.1 M HEPES pH 7.5, 22% w/v PEG Smear Broad). The crystal was flash-frozen in liquid nitrogen after soaking in reservoir solution supplemented with 20% glycerol as cryo-protectant. Data were collected at synchrotron beamline BioMAX, MAX IV Laboratory, Lund, Sweden, at 100 K and λ = 0.9763 Å. 3600 images were collected with an oscillation range of 0.1° per image. The beamline is equipped with an Eiger 16 M hybrid-pixel detector. Data extending to 2.2 Å were processed using EDNA_proc[82] which includes the software XDS[76] and Aimless[77] Crystals consisted of a single molecule in the asymmetric unit (ASU) in $P3_1$ space group. A molecular replacement solution for the Fab was obtained by PHASER[79] using the previously disclosed crystal structure of the panitumumab WT CH1:Cκ Fab[54] The structures were built manually in COOT[80] and refined using PHENIX[81] to a final to a final R and R_{free} of 18.0% and 23.0%, respectively. Coordinates and structure factors have been deposited in the PDB under accession code 9MI7.

Acknowledgments

We thank our colleagues Joseph Warfield, Kevin Schutz, Max Vasquez, Juergen Nett, Eric Krauland, Jessica Dawson, Amy Bray, and Chris Sullivan for their assistance on the project and in editing the manuscript. We thank the High Throughput Expression and Protein Analytics groups at Adimab for their data collection efforts and generation of constructs.

Disclosure statement

The authors are current or past employees of Adimab, LLC and may hold shares in Adimab, LLC. K.B., A.S., and M.B.B. are authors on patents and patent applications describing heavy/light chain pairing mutations.

Funding

The author(s) reported there is no funding associated with the work featured in this article.

ORCID

Kyle A. Barlow http://orcid.org/0000-0002-9787-0066
Michael B. Battles http://orcid.org/0000-0002-5321-7460
C. Garrett Rappazzo http://orcid.org/0000-0002-8415-444X

Data availability statement

Coordinates for the Fab containing the 1443 mutation set have been deposited in the Protein Data Bank under accession code 9MFN. Coordinates for the Fab containing the 1993 mutation set have been deposited in the Protein Data Bank under accession code 9MI7.

Abbreviations

AA	amino acid
AC-SINS	affinity-capture self-interaction nanoparticle spectroscopy
bsAb	bispecific antibody
CEX	cation exchange chromatography
cFAE	controlled Fab arm exchange
C_H1	IgG1 wild-type constant domain
cLC	common light chain
Cκ	light chain wild-type kappa constant domain
DID	double interface design
Fab	fragment antigen-binding region
HC	heavy chain
HIC	hydrophobic interaction chromatography
K_D	dissociation constant
KiH	knob-into-hole
LC-MS	liquid chromatography-mass spectrometry
LC	light chain
PDB	Protein Data Bank
PSR	polyspecificity reagent
RHS	Rosetta heterodimerization score
SEC	size exclusion chromatography
SID	single interface design
V_H	heavy chain variable domain
Vκ	light chain variable domain
WT	wildtype

References

1. The Antibody Society. Therapeutic monoclonal antibodies approved or in regulatory review [Internet]. [accessed 2024 Aug

1]. https://www.antibodysociety.org/antibody-therapeutics-product-data/.
2. Labrijn AF, Janmaat ML, Reichert JM, Parren PWHI. Bispecific antibodies: a mechanistic review of the pipeline. Nat Rev Drug Discov. 2019;18(8):585–608. doi: 10.1038/s41573-019-0028-1.
3. Kaplon H, Chenoweth A, Crescioli S, Reichert JM. Antibodies to watch in 2022. Mabs. 2022;14(1):2014296. doi: 10.1080/19420862.2021.2014296.
4. Kaplon H, Crescioli S, Chenoweth A, Reichert JV, Reichert JM. Antibodies to watch in 2023. mAbs. 2023;15(1). doi: 10.1080/19420862.2022.2153410.
5. Mullard A. FDA approves 100th monoclonal antibody product. Nat Rev Drug Discov. 2021;20(7):491–495. doi: 10.1038/d41573-021-00079-7.
6. Brinkmann U, Kontermann RE. The making of bispecific antibodies. Mabs. 2017;9(2):182–212. doi: 10.1080/19420862.2016.1268307.
7. Schaefer W, Regula JT, Bähner M, Schanzer J, Croasdale R, Dürr H, Gassner C, Georges G, Kettenberger H, Imhof-Jung S, et al. Immunoglobulin domain crossover as a generic approach for the production of bispecific IgG antibodies. Proc Natl Acad Sci. 2011;108(27):11187–11192. doi: 10.1073/pnas.1019002108.
8. Sampei Z, Igawa T, Soeda T, Okuyama-Nishida Y, Moriyama C, Wakabayashi T, Tanaka E, Muto A, Kojima T, Kitazawa T, et al. Identification and multidimensional optimization of an asymmetric bispecific IgG antibody mimicking the function of factor VIII cofactor activity. PLOS ONE. 2013;8(2):e57479. doi: 10.1371/journal.pone.0057479.
9. Blarcom TV, Lindquist K, Melton Z, Cheung WL, Wagstrom C, McDonough D, Oseguera CV, Ding S, Rossi A, Potluri S, et al. Productive common light chain libraries yield diverse panels of high affinity bispecific antibodies. Mabs. 2017;10(2):256–268. doi: 10.1080/19420862.2017.1406570.
10. Sharkey B, Pudi S, Moyer IW, Zhong L, Prinz B, Baruah H, Lynaugh H, Kumar S, Wittrup KD, Nett JH. Purification of common light chain IgG-like bispecific antibodies using highly linear pH gradients. mAbs. 2017;9(2):257–268. doi: 10.1080/19420862.2016.1267090.
11. Geuijen C, Tacken P, Wang L-C, Klooster R, van Loo PF, Zhou J, Mondal A, Liu Y, Kramer A, Condamine T, et al. A human CD137×PD-L1 bispecific antibody promotes anti-tumor immunity via context-dependent T cell costimulation and checkpoint blockade. Nat Commun. 2021;12(1):4445. doi: 10.1038/s41467-021-24767-5.
12. Ching KH, Berg K, Reynolds K, Pedersen D, Macias A, Abdiche YN, Harriman WD, Leighton PA. Common light chain chickens produce human antibodies of high affinity and broad epitope coverage for the engineering of bispecifics. mAbs. 2021;13(1):1862451. doi: 10.1080/19420862.2020.1862451.
13. Harris KE, Aldred SF, Davison LM, Ogana HAN, Boudreau A, Brüggemann M, Osborn M, Ma B, Buelow B, Clarke SC, et al. Sequence-based discovery demonstrates that fixed light chain human transgenic rats produce a diverse repertoire of antigen-specific antibodies. Front Immunol. 2018;9:889. doi: 10.3389/fimmu.2018.00889.
14. Labrijn AF, Meesters JI, Priem P, de Jong RN, van den Bremer ETJ, van Kampen MD, Gerritsen AF, Schuurman J, Parren PWHI. Controlled Fab-arm exchange for the generation of stable bispecific IgG1. Nat Protoc. 2014;9(10):2450–2463. doi: 10.1038/nprot.2014.169.
15. Dillon M, Yin Y, Zhou J, McCarty L, Ellerman D, Slaga D, Junttila TT, Han G, Sandoval W, Ovacik MA, et al. Efficient production of bispecific IgG of different isotypes and species of origin in single mammalian cells. Mabs. 2017;9(2):213–230. doi: 10.1080/19420862.2016.1267089.
16. Ovacik AM, Li J, Lemper M, Danilenko D, Stagg N, Mathieu M, Ellerman D, Gupta V, Kalia N, Nguy T, et al. Single cell-produced and in vitro-assembled anti-FcRH5/CD3 T-cell dependent bispecific antibodies have similar in vitro and in vivo properties. Mabs. 2019;11(2):422–433. doi: 10.1080/19420862.2018.1551676.
17. Koga H, Yamano T, Betancur J, Nagatomo S, Ikeda Y, Yamaguchi K, Nabuchi Y, Sato K, Teranishi-Ikawa Y, Sato M, et al. Efficient production of bispecific antibody by FAST-IgTM and its application to NXT007 for the treatment of hemophilia a. mAbs. 2023;15(1):2222441. doi: 10.1080/19420862.2023.2222441.
18. Joshi KK, Phung W, Han G, Yin Y, Kim I, Sandoval W, Carter PJ. Elucidating heavy/light chain pairing preferences to facilitate the assembly of bispecific IgG in single cells. Mabs. 2019;11(7):1254–1265. doi: 10.1080/19420862.2019.1640549.
19. Herold EM, John C, Weber B, Kremser S, Eras J, Berner C, Deubler S, Zacharias M, Buchner J. Determinants of the assembly and function of antibody variable domains. Sci Rep-UK. 2017;7(1):12276. doi: 10.1038/s41598-017-12519-9.
20. Röthlisberger D, Honegger A, Plückthun A. Domain interactions in the fab fragment: a comparative evaluation of the single-chain Fv and Fab format engineered with variable domains of different stability. J Mol Biol. 2005;347(4):773–789. doi: 10.1016/j.jmb.2005.01.053.
21. Toughiri R, Wu X, Ruiz D, Huang F, Crissman JW, Dickey M, Froning K, Conner EM, Cujec TP, Demarest SJ. Comparing domain interactions within antibody Fabs with kappa and lambda light chains. Mabs. 2016;8(7):1276–1285. doi: 10.1080/19420862.2016.1214785.
22. Teerinen T, Valjakka J, Rouvinen J, Takkinen K. Structure-based stability engineering of the mouse IgG1 Fab fragment by modifying constant domains. J Mol Biol. 2006;361(4):687–697. doi: 10.1016/j.jmb.2006.06.073.
23. Pomarici ND, Waibl F, Quoika PK, Bujotzek A, Georges G, Fernández-Quintero ML, Liedl KR. Structural mechanism of Fab domain dissociation as a measure of interface stability. J Comput Aid Mol Des. 2023;37(4):201–215. doi: 10.1007/s10822-023-00501-9.
24. Lewis SM, Wu X, Pustilnik A, Sereno A, Huang F, Rick HL, Guntas G, Leaver-Fay A, Smith EM, Ho C, et al. Generation of bispecific IgG antibodies by structure-based design of an orthogonal Fab interface. Nat Biotechnol. 2014;32(2):191–198. doi: 10.1038/nbt.2797.
25. Froning KJ, Leaver-Fay A, Wu X, Phan S, Gao L, Huang F, Pustilnik A, Bacica M, Houlihan K, Chai Q, et al. Computational design of a specific heavy chain/κ light chain interface for expressing fully IgG bispecific antibodies. Protein Sci. 2017;26(10):2021–2038. doi: 10.1002/pro.3240.
26. Feige MJ, Hendershot LM, Buchner J. How antibodies fold. Trends Biochem Sci. 2010;35(4):189–198. doi: 10.1016/j.tibs.2009.11.005.
27. Mazor Y, Oganesyan V, Yang C, Hansen A, Wang J, Liu H, Sachsenmeier K, Carlson M, Gadre DV, Borrok MJ, et al. Improving target cell specificity using a novel monovalent bispecific IgG design. Mabs. 2015;7(2):377–389. doi: 10.1080/19420862.2015.1007816.
28. Golay J, Choblet S, Iwaszkiewicz J, Cérutti P, Ozil A, Loisel S, Pugnière M, Ubiali G, Zoete V, Michielin O, et al. Design and validation of a novel generic platform for the production of tetravalent IgG1-like bispecific antibodies. J Immunol. 2016;196(7):3199–3211. doi: 10.4049/jimmunol.1501592.
29. Iwasaki YW, Tharakaraman K, Subramanian V, Khongmanee A, Hatas A, Fleischer E, Rurak TT, Ngok-Ngam P, Tit-Oon P, Ruchirawat M, et al. Generation of bispecific antibodies by structure-guided redesign of IgG constant regions. Front Immunol. 2023;13:1063002. doi: 10.3389/fimmu.2022.1063002.
30. Joachimiak LA, Kortemme T, Stoddard BL, Baker D. Computational design of a new hydrogen bond network and at least a 300-fold specificity switch at a protein–protein interface. J Mol Biol. 2006;361(1):195–208. doi: 10.1016/j.jmb.2006.05.022.
31. Kortemme T, Joachimiak LA, Bullock AN, Schuler AD, Stoddard BL, Baker D. Computational redesign of protein-protein interaction specificity. Nat Struct Mol Biol. 2004;11(4):371–379. doi: 10.1038/nsmb749.
32. Maguire JB, Boyken SE, Baker D, Kuhlman B. Rapid sampling of hydrogen bond networks for computational protein design.

J Chem Theory Comput. 2018;14(5):2751–2760. doi: 10.1021/acs.jctc.8b00033.
33. Boyken SE, Chen Z, Groves B, Langan RA, Oberdorfer G, Ford A, Gilmore JM, Xu C, DiMaio F, Pereira JH, et al. De Novo design of protein homo-oligomers with modular hydrogen-bond network–mediated specificity. Science. 2016;352(6286):680–687. doi: 10.1126/science.aad8865.
34. Barlow KA, Conchúir SO, Thompson S, Suresh P, Lucas JE, Heinonen M, Kortemme T. Flex ddG: Rosetta ensemble-based estimation of changes in protein–protein binding affinity upon mutation. J Phys Chem B. 2018;122(21):5389–5399. doi: 10.1021/acs.jpcb.7b11367.
35. Keedy DA, Georgiev I, Triplett EB, Donald BR, Richardson DC, Richardson JS. The role of local backrub motions in evolved and designed mutations. PLOS Comput Biol. 2012;8(8):e1002629. doi: 10.1371/journal.pcbi.1002629.
36. Davis IW, Arendall WB, Richardson DC, Richardson JS. The backrub motion: how protein backbone shrugs when a sidechain dances. Structure. 2006;14(2):265–274. doi: 10.1016/j.str.2005.10.007.
37. Smith CA, Kortemme T. Backrub-like backbone simulation recapitulates natural protein conformational variability and improves mutant side-chain prediction. J Mol Biol. 2008;380(4):742–756. doi: 10.1016/j.jmb.2008.05.023.
38. Ridgway JBB, Presta LG, Carter P. 'Knobs-into-holes' engineering of antibody CH3 domains for heavy chain heterodimerization. Protein Eng, Des Sel. 1996;9(7):617–621. doi: 10.1093/protein/9.7.617.
39. Merchant AM, Zhu Z, Yuan JQ, Goddard A, Adams CW, Presta LG, Carter P. An efficient route to human bispecific IgG. Nat Biotechnol. 1998;16(7):677–681. doi: 10.1038/nbt0798-677.
40. Atwell S, Ridgway JBB, Wells JA, Carter P. Stable heterodimers from remodeling the domain interface of a homodimer using a phage display library11Edited by P.E.Wright. J Mol Biol. 1997;270(1):26–35. doi: 10.1006/jmbi.1997.1116.
41. Poskute R, Sankaran PK, Sewell L, Lepore G, Shrubsall R, Dewis L, Watanabe Y, Wong V, Fernandez LP, Mishra R, et al. Identification and quantification of chain-pairing variants or mispaired species of asymmetric monovalent bispecific IgG1 monoclonal antibody format using reverse-phase polyphenyl chromatography coupled electrospray ionization mass spectrometry. J Chromatogr B. 2024;1237:124085. doi: 10.1016/j.jchromb.2024.124085.
42. Wang C, Vemulapalli B, Cao M, Gadre D, Wang J, Hunter A, Wang X, Liu D. A systematic approach for analysis and characterization of mispairing in bispecific antibodies with asymmetric architecture. mAbs. 2018;10(8):1226–1235. doi: 10.1080/19420862.2018.1511198.
43. Jain T, Sun T, Durand S, Hall A, Houston NR, Nett JH, Sharkey B, Bobrowicz B, Caffry I, Yu Y, et al. Biophysical properties of the clinical-stage antibody landscape. Proc Natl Acad Sci. 2017;114(5):944–949. doi: 10.1073/pnas.1616408114.
44. Xu Y, Roach W, Sun T, Jain T, Prinz B, Yu T-Y, Torrey J, Thomas J, Bobrowicz P, Vásquez M, et al. Addressing polyspecificity of antibodies selected from an in vitro yeast presentation system: a FACS-based, high-throughput selection and analytical tool. Protein Eng Des Sel. 2013;26(10):663–670. doi: 10.1093/protein/gzt047.
45. Shehata L, Maurer DP, Wec AZ, Lilov A, Champney E, Sun T, Archambault K, Burnina I, Lynaugh H, Zhi X, et al. Affinity maturation enhances antibody specificity but compromises conformational stability. Cell Rep. 2019;28(13):3300–3308.e4. doi: 10.1016/j.celrep.2019.08.056.
46. Kelly RL, Geoghegan JC, Feldman J, Jain T, Kauke M, Le D, Zhao J, Wittrup KD. Chaperone proteins as single component reagents to assess antibody nonspecificity. Mabs. 2017;9(7):1036–1040. doi: 10.1080/19420862.2017.1356529.
47. Kunert R, Reinhart D. Advances in recombinant antibody manufacturing. Appl Microbiol Biotechnol. 2016;100(8):3451–3461. doi: 10.1007/s00253-016-7388-9.
48. Liu Y, Caffry I, Wu J, Geng SB, Jain T, Sun T, Reid F, Cao Y, Estep P, Yu Y, et al. High-throughput screening for developability during early-stage antibody discovery using self-interaction nanoparticle spectroscopy. Mabs. 2013;6(2):483–492. doi: 10.4161/mabs.27431.
49. Cohen S, Chung S, Spiess C, Lundin V, Stefanich E, Laing ST, Clark V, Brumm J, Zhou Y, Huang C, et al. An integrated approach for characterizing immunogenic responses toward a bispecific antibody. Mabs. 2021;13(1):1944017. doi: 10.1080/19420862.2021.1944017.
50. Jawa V, Terry F, Gokemeijer J, Mitra-Kaushik S, Roberts BJ, Tourdot S, Groot ASD. T-Cell dependent immunogenicity of protein therapeutics pre-clinical assessment and mitigation–updated consensus and review 2020. Front Immunol. 2020;11:1301. doi: 10.3389/fimmu.2020.01301.
51. Cohen S, Myneni S, Batt A, Guerrero J, Brumm J, Chung S. Immunogenicity risk assessment for biotherapeutics through in vitro detection of CD134 and CD137 on T helper cells. Mabs. 2021;13(1):1898831. doi: 10.1080/19420862.2021.1898831.
52. Gonzalez-Galarza FF, McCabe A, dos Santos EJM, Jones J, Takeshita L, Ortega-Rivera ND, Cid-Pavon GMD, Ramsbottom K, Ghattaoraya G, Alfirevic A, et al. Allele frequency net database (AFND) 2020 update: gold-standard data classification, open access genotype data and new query tools. Nucleic Acids Res. 2019;48:D783–8. doi: 10.1093/nar/gkz1029.
53. Walsh RE, Lannan M, Wen Y, Wang X, Moreland CA, Willency J, Knierman MD, Spindler L, Liu L, Zeng W, et al. Post-hoc assessment of the immunogenicity of three antibodies reveals distinct immune stimulatory mechanisms. Mabs. 2020;12(1):1764829. doi: 10.1080/19420862.2020.1764829.
54. Sickmier EA, Kurzeja RJM, Michelsen K, Vazir M, Yang E, Tasker AS. The panitumumab EGFR complex reveals a binding mechanism that overcomes cetuximab induced resistance. PLOS ONE. 2016;11(9):e0163366. doi: 10.1371/journal.pone.0163366.
55. Crescioli S, Kaplon H, Chenoweth A, Wang L, Visweswaraiah J, Reichert JM. Antibodies to watch in 2024. mAbs. 2024;16(1):2297450. doi: 10.1080/19420862.2023.2297450.
56. Liu CY, Ahonen CL, Brown ME, Zhou L, Welin M, Krauland EM, Pejchal R, Widboom PF, Battles MB. Structure-based engineering of a novel CD3ε-targeting antibody for reduced polyreactivity. Mabs. 2023;15(1):2189974. doi: 10.1080/19420862.2023.2189974.
57. Stranges PB, Kuhlman B. A comparison of successful and failed protein interface designs highlights the challenges of designing buried hydrogen bonds. Protein Sci. 2013;22(1):74–82. doi: 10.1002/pro.2187.
58. Sammond DW, Eletr ZM, Purbeck C, Kuhlman B. Computational design of second-site suppressor mutations at protein–protein interfaces. Proteins Struct Funct Bioinform. 2010;78(4):1055–1065. doi: 10.1002/prot.22631.
59. Bermeo S, Favor A, Chang Y-T, Norris A, Boyken SE, Hsia Y, Haddox HK, Xu C, Brunette TJ, Wysocki VH, et al. De Novo design of obligate abc-type heterotrimeric proteins. Nat Struct Mol Biol. 2022;29(12):1266–1276. doi: 10.1038/s41594-022-00879-4.
60. Chen Z, Boyken SE, Jia M, Busch F, Flores-Solis D, Bick MJ, Lu P, VanAernum ZL, Sahasrabuddhe A, Langan RA, et al. Programmable design of orthogonal protein heterodimers. Nature. 2019;565(7737):106–111. doi: 10.1038/s41586-018-0802-y.
61. Fernández-Quintero ML, Quoika PK, Wedl FS, Seidler CA, Kroell KB, Loeffler JR, Pomarici ND, Hoerschinger VJ, Bujotzek A, Georges G, et al. Comparing antibody interfaces to inform rational design of new antibody formats. Front Mol Biosci. 2022;9:812750. doi: 10.3389/fmolb.2022.812750.
62. Schmitt C, Emrich T, Chebon S, Fernandez E, Petry C, Yoneyama K, Kiialainen A, Howard M, Niggli M, Paz-Priel I, et al. Low immunogenicity of emicizumab in persons with haemophilia a. Haemophilia. 2021;27(6):984–992. doi: 10.1111/hae.14398.
63. Zhou Y, Penny HL, Kroenke MA, Bautista B, Hainline K, Chea LS, Parnes J, Mytych DT. Immunogenicity assessment of bispecific

antibody-based immunotherapy in oncology. J Immunother Cancer. 2022;10(4):10. doi: 10.1136/jitc-2021-004225.
64. Hosseini I, Gadkar K, Stefanich E, Li C-C, Sun LL, Chu Y-W, Ramanujan S. Mitigating the risk of cytokine release syndrome in a phase I trial of CD20/CD3 bispecific antibody mosunetuzumab in NHL: impact of translational system modeling. Npj Syst Biol Appl. 2020;6(1):28. doi: 10.1038/s41540-020-00145-7.
65. Hellmann MD, Bivi N, Calderon B, Shimizu T, Delafontaine B, Liu ZT, Szpurka AM, Copeland V, Hodi FS, Rottey S, et al. Safety and immunogenicity of LY3415244, a bispecific antibody against TIM-3 and PD-L1, in patients with advanced solid tumors. Clin Cancer Res. 2021;27(10):2773–2781. doi: 10.1158/1078-0432.CCR-20-3716.
66. Staton TL, Peng K, Owen R, Choy DF, Cabanski CR, Fong A, Brunstein F, Alatsis KR, Chen H. A phase I, randomized, observer-blinded, single and multiple ascending-dose study to investigate the safety, pharmacokinetics, and immunogenicity of BITS7201A, a bispecific antibody targeting IL-13 and IL-17, in healthy volunteers. BMC Pulm Med. 2019;19(1):5. doi: 10.1186/s12890-018-0763-9.
67. Bivi N, Moore T, Rodgers G, Denning H, Shockley T, Swearingen CA, Gelfanova V, Calderon B, Peterson DA, Hodsdon ME, et al. Investigation of pre-existing reactivity to biotherapeutics can uncover potential immunogenic epitopes and predict immunogenicity risk. Mabs. 2019;11(5):861–869. doi: 10.1080/19420862.2019.1612699.
68. FDA. Bispecific antibody development programs guidance for industry [Internet]. 2021 [accessed 2024 May 15]. https://www.fda.gov/regulatory-information/search-fda-guidance-documents/bispecific-antibody-development-programs-guidance-industry.
69. Leaver-Fay A, O'Meara MJ, Tyka M, Jacak R, Song Y, Kellogg EH, Thompson J, Davis IW, Pache RA, Lyskov S, et al. Chapter six scientific benchmarks for guiding macromolecular energy function improvement. Methods Enzym. 2013;523:109–143.
70. O'Meara MJ, Leaver-Fay A, Tyka MD, Stein A, Houlihan K, DiMaio F, Bradley P, Kortemme T, Baker D, Snoeyink J, et al. Combined covalent-electrostatic model of hydrogen bonding improves structure prediction with Rosetta. J Chem Theory Comput. 2015;11(2):609–622. doi: 10.1021/ct500864r.
71. Boder ET, Wittrup KD. Yeast surface display for screening combinatorial polypeptide libraries. Nat Biotechnol. 1997;15(6):553–557. doi: 10.1038/nbt0697-553.
72. Blaise L, Wehnert A, Steukers MPG, van den Beucken T, Hoogenboom HR, Hufton SE. Construction and diversification of yeast cell surface displayed libraries by yeast mating: application to the affinity maturation of Fab antibody fragments. Gene. 2004;342(2):211–218. doi: 10.1016/j.gene.2004.08.014.
73. Sazinsky SL, Ott RG, Silver NW, Tidor B, Ravetch JV, Wittrup KD. Aglycosylated immunoglobulin G1 variants productively engage activating Fc receptors. Proc Natl Acad Sci. 2008;105(51):20167–20172. doi: 10.1073/pnas.0809257105.
74. Estep P, Caffry I, Yu Y, Sun T, Cao Y, Lynaugh H, Jain T, Vásquez M, Tessier PM, Xu Y. An alternative assay to hydrophobic interaction chromatography for high-throughput characterization of monoclonal antibodies. mAbs. 2015;7(3):553–561. doi: 10.1080/19420862.2015.1016694.
75. Sule SV, Sukumar M, Weiss WF, Marcelino-Cruz AM, Sample T, Tessier PM. High-throughput analysis of concentration-dependent antibody self-association. Biophys J. 2011;101(7):1749–1757. doi: 10.1016/j.bpj.2011.08.036.
76. Kabsch W. XDS. Acta Crystallogr Sect D Biol Crystallogr. 2010;66(2):125–132. doi: 10.1107/S0907444909047337.
77. Evans PR, Murshudov GN. How good are my data and what is the resolution? Acta Crystallogr Sect D. 2013;69(7):1204–1214. doi: 10.1107/S0907444913000061.
78. Winn MD, Ballard CC, Cowtan KD, Dodson EJ, Emsley P, Evans PR, Keegan RM, Krissinel EB, Leslie AGW, McCoy A, et al. Overview of the CCP4 suite and current developments. Acta Crystallogr Sect D. 2011;67(4):235–242. doi: 10.1107/S0907444910045749.
79. McCoy AJ, Grosse-Kunstleve RW, Adams PD, Winn MD, Storoni LC, Read RJ. Phaser crystallographic software. J Appl Crystallogr. 2007;40(4):658–674. doi: 10.1107/S0021889807021206.
80. Emsley P, Lohkamp B, Scott WG, Cowtan K. Features and development of coot. Acta Crystallogr Sect D Biol Crystallogr. 2010;66(4):486–501. doi: 10.1107/S0907444910007493.
81. Adams PD, Afonine PV, Bunkóczi G, Chen VB, Davis IW, Echols N, Headd JJ, Hung L-W, Kapral GJ, Grosse-Kunstleve RW, et al. PHENIX: a comprehensive python-based system for macromolecular structure solution. Acta Crystallogr Sect D Biol Crystallogr. 2010;66(2):213–221. doi: 10.1107/S0907444909052925.
82. Monaco S, Gordon E, Bowler MW, Delagenière S, Guijarro M, Spruce D, Svensson O, McSweeney SM, McCarthy AA, Leonard G, et al. Automatic processing of macromolecular crystallography X-ray diffraction data at the ESRF. J Appl Crystallogr. 2013;46(3):804–810. doi: 10.1107/S0021889813006195.